Supplementary Information

Ether-Functionalized Asymmetric Lithium Imide Salts: Molecular Design Principles for Low-Melting Molten Salt Electrolytes

Yuna Matsuyama,[a] Ayaka Hisamune,[a] Taku Sudoh,[a] Md. Sharif Hossain,[a,b] Seiji Tsuzuki,[c] Frederik Philippi,[d]* Kazuhide Ueno [a,c]*

[a] *Department of Chemistry and Life Science, Yokohama National University, 79-5 Tokiwadai, Hodogaya-ku, Yokohama, Kanagawa, 240-8501, Japan*
[b] *Chemical Engineering Department, Kanagawa Institiute of Industrial Science and Technology, 705-1 Shimoimaizumi, Ebina, Kanagawa, 243-0435, Japan*
[c] *Institute of Advanced Science, Yokohama National University, 79-5 Tokiwadai, Hodogaya-ku, Yokohama, Kanagawa, 240-8501, Japan*
[d] *Laboratoire de Chimie ENS de Lyon, Campus Monod Room M6.056, 46 Allée d 'Italie, 69364 Lyon Cedex 07, France*

Synthetic Procedures

All the reactions were conducted using Schlenk techniques.[1]

H[TfN5], Li[TfN5], H[TfN3O1] and Li[TfN3O1] were prepared as described previously.[2]

H[TfN2O2O2]: (2-(2-ethoxyethoxy)ethyl)((trifluoromethyl)sulfonyl)imide

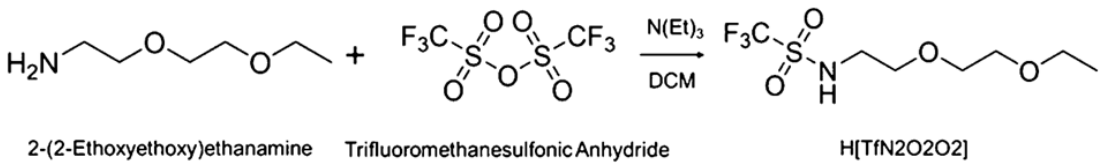

2-(2-ethoxyethoxy)ethanamine (9.93 g, 75 mmol, 1.00 equiv.) and triethylamine (15.8 mL, 11.46 g, 113 mmol, 1.52 equiv.) were dissolved in 180 mL of dry dichloromethane at −78 °C in a dry ice bath under Schlenk conditions. Then, a solution of trifluoromethanesulfonic anhydride (14.5 mL, 24.26 g, 86 mmol, 1.15 equiv.) in 80 mL of dry dichloromethane was added dropwise at approximately 1.5 mL/min. After the addition was complete, the mixture was allowed to reach room temperature and was stirred for an additional 5 h. The solvent (dichloromethane) was removed using a rotary evaporator, yielding a colorless, transparent liquid. To the residue, 35 mL of 4 M NaOH was added, followed by washing with dichloromethane (40 mL×3). Subsequently, the aqueous phase was then acidified with 6 M HCl (40 mL), followed by extraction with dichloromethane (40 mL × 3). The combined organic layers were dried over $MgSO_4$, and concentrated under reduced pressure using a rotary evaporator. Vacuum distillation (oil bath: ~65 °C, 0.04 mbar) gave 12.82 g of a colorless, transparent liquid: 2-(2-ethoxyethoxy)ethyl((trifluoromethyl)sulfonyl)imide (**H[TfN2O2O2]**) (48.3 mmol, 65 % isolated yield).

^{1}H NMR (DMSO-d_6, 500 MHz, δ in ppm): 9.47 (t, $^3J_{H/H}$ = 10.3 Hz 1H, N-***H***), 3.53-3.46 (m, 6H, C***H***$_2$-O-C$_2$***H***$_4$-O), 3.43 (t, $^3J_{H/H}$ = 14.3 Hz, 2H, N-C***H***$_2$), 3.27 (q, $^3J_{H/H}$ = 16.6 Hz, 2H, -C***H***$_2$CH$_3$), 1.09 (t, $^3J_{H/H}$ = 13.8 Hz, 3H, -C***H***$_3$) . ^{13}C{^{1}H} NMR (DMSO-d_6, 126 MHz, δ in ppm): 120.15 (q, $^1J_{C/F}$ = 322.7 Hz, ***C***F$_3$), 70.26 (s, N- ***C***H$_2$), 69.66 (s, N-CH$_2$-***C***H$_2$), 69.52 (s, N-C$_2$H$_4$-O-***C***$_2$H$_4$), 66.09 (s, N-C$_2$H$_4$- O-***C***$_2$H$_4$), 43.76 (s, ***C***H$_2$-CH$_3$), 15.59 (s, ***C***H$_3$). ^{19}F NMR (DMSO-d_6, 471 MHz, δ in ppm): −77.32 (s, C***F***$_3$).

Li[TfN2O2O2]: Lithium(2-(2-ethoxyethoxy)ethyl)((trifluoromethyl)sulfonyl)imide

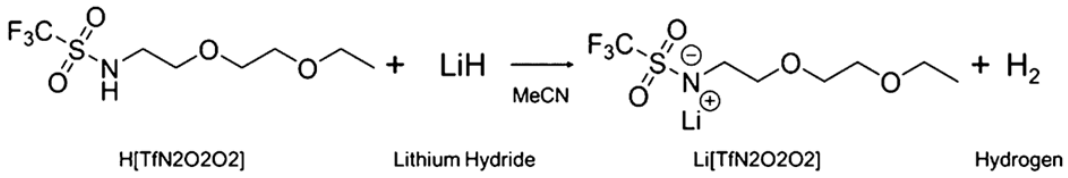

Lithium hydride (0.319 g, 40 mmol, 1.50 equiv.) was dispersed in 50 mL of dry acetonitrile in a 100 mL Schlenk flask. While cooling the suspension in an ice bath, 2-(2-ethoxyethoxy)ethyl((trifluoromethyl)sulfonyl)imide (7.00 g, 26 mmol, 1.00 equiv.) was added slowly. After the addition, the reaction mixture was stirred for 2 h, then transferred by filtration through a filter cannula (glass fiber filter paper, Teflon tape, and a PTFE cannula) into another Schlenk flask. Removal of the solvent afforded a solid, which was further dried under vacuum at 65 °C to give lithium(2-(2-ethoxyethoxy)ethyl)((trifluoromethyl)sulfonyl)imide (**Li[TfN2O2O2**]) as a solid (2.18 g, 8.04 mmol, 30% isolated yield).

^{1}H NMR (DMSO-d_6, 500 MHz, δ in ppm): 3.46-3.25 (m, 8H, $C_2\boldsymbol{H}_4$-O-$C_2\boldsymbol{H}_4$-O), 3.27 (q, $^{3}J_{H/H}$ = 14.7 Hz, 2H, C$\boldsymbol{H}_2$-CH_3), 1.08 (t, $^{3}J_{H/H}$ = 13.7 Hz, 3H, C$\boldsymbol{H}_3$). ^{13}C{^{1}H} NMR (DMSO-d_6, 101 MHz, δ in ppm): 123.41 (q, $^{1}J_{C/F}$ = 334.5 Hz, $\boldsymbol{C}F_3$), 73.64 (s, N- $\boldsymbol{C}H_2$), 70.13 (s, N-CH_2-$\boldsymbol{C}H_2$), 69.82 (s, N-C_2H_4-O-$\boldsymbol{C}_2H_4$), 66.05(s, N-C_2H_4- O-$\boldsymbol{C}_2H_4$), 46.05 (s, $\boldsymbol{C}H_2$-CH_3), 15.66 (s, $\boldsymbol{C}H_3$). ^{19}F NMR (DMSO-d_6, 471 MHz, δ in ppm): −75.69 (s, C$\boldsymbol{F}_3$). ESI-MS (negative ion mode): m/z calculated for $[TfN2O2O2]^-$ = 264.24; found = 264.05.

H[TfN7]: heptyl((trifluoromethyl)sulfonyl)imide

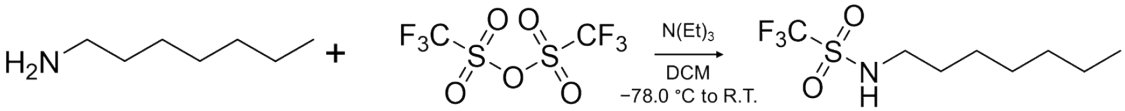

^{1}H NMR (DMSO-d_6, 500 MHz, δ in ppm): 9.21 (s, 1H, N-$\boldsymbol{H}$), 3.10 (t, $^{3}J_{H/H}$ = 14.3 Hz, 2H, N-C$\boldsymbol{H}_2$), 1.49 (quin, $^{3}J_{H/H}$ = 28.6 Hz, 2H, -C$\boldsymbol{H}_2$$CH_3$), 1.29-1.19 (m, 8H, -$C_4\boldsymbol{H}_8CH_3$), 0.85 (t, $^{3}J_{H/H}$ = 14.3 Hz, 3H, C$\boldsymbol{H}_3$). ^{13}C{^{1}H} NMR (DMSO-d_6, 126 MHz, δ in ppm): 123.55 (q, $^{1}J_{C/F}$ = 334.7 Hz, $\boldsymbol{C}F_3$), 46.21 (s, N- $\boldsymbol{C}H_2$), 33.59 (s, N-CH_2-$\boldsymbol{C}H_2$), 32.00 (s, N-C_2H_4- $\boldsymbol{C}H_2$), 29.26 (s, N-C_3H_6 -$\boldsymbol{C}H_2$), 27.30 (s, $\boldsymbol{C}H_2$-C_2H_5), 22.65 (s, $\boldsymbol{C}H_2$-CH_3), 14.48 (s, $\boldsymbol{C}H_3$). ^{19}F NMR (DMSO-d_6, 471 MHz, δ in ppm): −77.98 (s, C$\boldsymbol{F}_3$).

Li[TfN7]: Lithium (heptyl)((trifluoromethyl)sulfonyl)imide

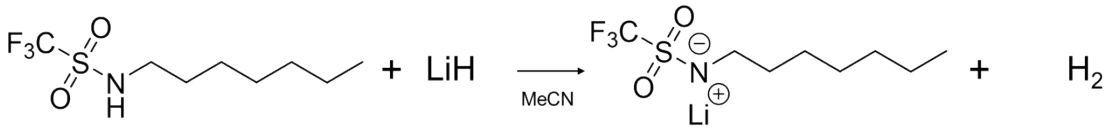

^{1}H NMR (DMSO-d$_6$, 500 MHz, δ in ppm): 2.81 (s, 2H, N-C***H***$_2$), 1.25 (quin, $^{3}J_{H/H}$ = 34.9 Hz, 10H, -C$_5$***H***$_{10}$), 0.84 (t, $^{3}J_{H/H}$ = 13.8 Hz, 3H, C***H***$_3$). ^{13}C{^{1}H} NMR (DMSO-d$_6$, 126 MHz, δ in ppm): 123.59 (q, $^{1}J_{C/F}$ = 335.9 Hz, ***C***F$_3$), 46.24 (s, N- ***C***H$_2$), 33.62 (s, N-CH$_2$-***C***H$_2$), 32.00 (s, N-C$_2$H$_4$- ***C***H$_2$), 29.27 (s, N-C$_3$H$_6$ -***C***H$_2$), 27.31 (s, ***C***H$_2$-C$_2$H$_5$), 22.66 (s, ***C***H$_2$-CH$_3$), 14.53 (s, ***C***H$_3$). ^{19}F NMR (DMSO-d$_6$, 471 MHz, δ in ppm): −75.76 (s, C***F***$_3$).

H[TfN2O2]: (2-ethoxyethyl)((trifluoromethyl)sulfonyl)imide

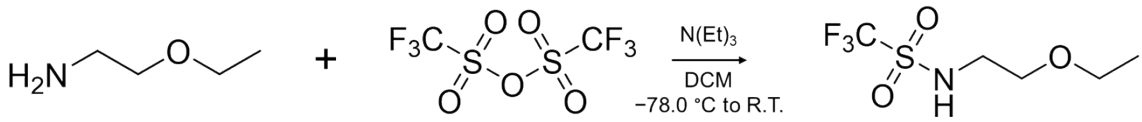

^{1}H NMR (DMSO-d$_6$, 500 MHz, δ in ppm): 9.48 (s, 1H, N-***H***), 3.46-3.42 (m, 4H, N-C***H***$_2$-CH$_2$O-C***H***$_2$), 3.27 (t, $^{3}J_{H/H}$ = 10.9 Hz, 2H, N-CH$_2$C***H***$_2$), 1.11 (t, $^{3}J_{H/H}$ = 14.3 Hz, 3H, C***H***$_3$). ^{13}C{^{1}H} NMR (DMSO-d$_6$, 126 MHz, δ in ppm): 120.15 (q, $^{1}J_{C/F}$ = 322.7 Hz, ***C***F$_3$), 68.83 (s, N- ***C***H$_2$), 66.00 (s, N-CH$_2$-***C***H$_2$), 43.82 (s, ***C***H$_2$-CH$_3$), 15.45 (s, ***C***H$_3$). ^{19}F NMR (DMSO-d$_6$, 471 MHz, δ in ppm): −77.29 (s, C***F***$_3$).

Li[TfN2O2]: Lithium(2-ethoxyethyl)((trifluoromethyl)sulfonyl)imide

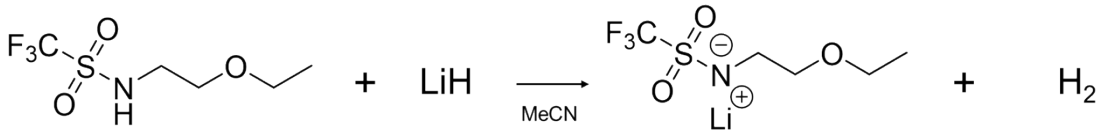

^{1}H NMR (DMSO-d$_6$, 400 MHz, δ in ppm): 3.36 (q, $^{3}J_{H/H}$ = 21.1 Hz, 2H, O-C***H***$_2$CH$_3$), 3.23 (t, $^{3}J_{H/H}$ = 14.7 Hz, 2H, N- C***H***$_2$), 2.96 (t, $^{3}J_{H/H}$ = 14.2 Hz, 2H, N-CH$_2$-C***H***$_2$), 1.05 (t, $^{3}J_{H/H}$ = 13.7 Hz, 3H, C***H***$_3$). ^{13}C{^{1}H} NMR (DMSO-d$_6$, 101 MHz, δ in ppm): 123.39 (q, $^{1}J_{C/F}$ = 334.5 Hz, ***C***F$_3$), 73.01 (s, N- ***C***H$_2$), 65.76 (s, N-CH$_2$-***C***H$_2$), 46.07 (s, ***C***H$_2$-CH$_3$), 15.73 (s, ***C***H$_3$). ^{19}F NMR (DMSO-d$_6$, 376 MHz, δ in ppm): −75.72 (s, C***F***$_3$).

H[MMP]:(N-(1-methoxymethyl)propyl)trifluoromethanesulfonyl)imide

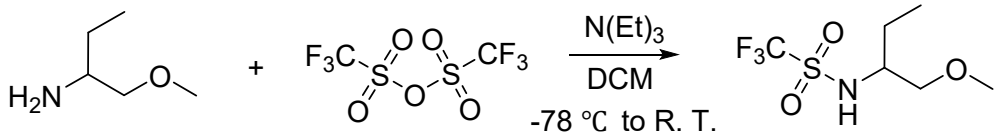

The same method used for synthesizing H[TfN2O2O2] was applied to prepare H[MMP] . In this case, 2-amino-1-1methoxybutane (9.63 g, 93 mmol, 1.00 equiv.), triethylamine (19.5 mL, 13.94 g, 138 mmol, 1.48 equiv.), and trifluoromethanesulfonic anhydride (15.9 mL, 27.42 g, 97 mmol, 1.04 equiv.) were used. The target product, (N-(1-methoxymethyl)propyl)trifluoromethanesulfonyl)imide(**H[MMP]**), was obtained in 26.5% isolated yield.

^{1}H NMR (DMSO-d_6, 500 MHz, δ in ppm): 9.253 (s, 1H, N-***H***), 3.36 (quin, $^{3}J_{H/H}$ = 24.63 Hz, 1H, N-C***H***), 3.32-3.27 (m, 3H, C***H***$_3$), 3.26 (s, 3H, C***H***$_3$-O-CH_2), 1.59-1.34 (m, 2H, N-CH-C***H***$_2$), 0.870-0.841(t, $^{3}J_{H/H}$ = 14.89 Hz, 3H, CH_2-C***H***$_3$).^{13}C{^{1}H} NMR (DMSO-d_6, 126 MHz, δ in ppm): 120.07 (q, $^{1}J_{C/F}$ = 322.7 Hz, ***C***F_3), 74.48 (s, N-CH-***C***H_2),58.78 (s, N-***C***H), 56.96 (s, O-***C***H_3), 25.02 (s, N-CH-***C***H_2), 10.33 (s, CH_2-***C***H_3).^{19}F NMR (DMSO-d_6, 471 MHz, δ in ppm): -77.61 (s, C***F***$_3$).

Li[MMP]: Lithium (N-(1-methoxymethyl)propyl)trifluoromethanesulfonyl)imide

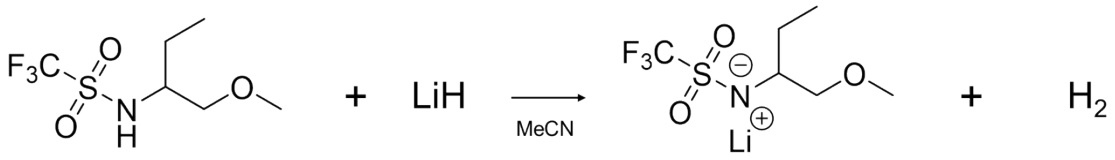

The same method used for synthesizing Li[TfN2O2O2] was applied to prepare Li[MMP]. Lithium hydride (0.12 g, 15 mmol, 1.36 equiv.) was reacted with (N-(1-methoxymethyl)propyl)trifluoromethanesulfonyl)imide(2.5 g, 11 mmol, 1.00 equiv.). The reaction yielded 1.41 g of Lithium (N-(1-methoxymethyl)propyl)trifluoromethanesulfonyl)imide (**Li[MMP]**) (5.84 mmol, 53% isolated yield).

^{1}H NMR (DMSO-d_6, 400 MHz, δ in ppm): 3.14 (s, 3H, O-C***H***$_3$), 3.10-3.04 (m, 1H, N-C***H***), 2.92(t, $^{3}J_{H/H}$=17.4 Hz, 1H, C***H***$_2$-O), 1.49-1.39, 1.10-0.10 (m, 2H, C***H***$_2$-CH_3), 0.78 (t, $^{3}J_{H/H}$ = 14.65 Hz, 3H, CH_2-C***H***$_3$).^{13}C{^{1}H} NMR (DMSO-d_6, 101 MHz, δ in ppm): 123. 38 (q, $^{1}J_{C/F}$ = 334 Hz, ***C***F_3), 78.39 (s, N-CH-***C***H_2), 58.48 (s, N-***C***H), 56.63 (s, O-***C***H_3), 27.77 (s, N-CH-***C***H_2), 10.52 (s, CH_2-***C***H_3).^{19}F NMR (DMSO-d_6, 376 MHz, δ in ppm): −75.89 (s, C***F***$_3$).

H[IESI]:(2-(isopropoxyethyl)trifluoromethanesulfonyl)imide

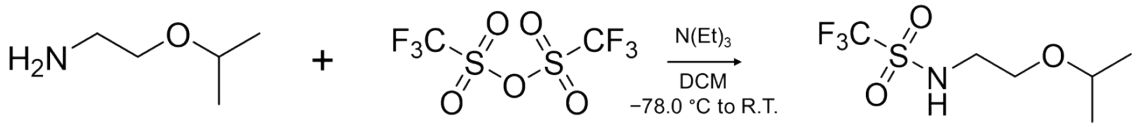

The same method used for synthesizing H[TfN2O2O2] was applied to prepare H[IESI] . In this case, 2-isopropoxyethylamine (8.92 g, 87 mmol, 1.00 equiv.), triethylamine (19.5 mL, 13.18 g, 130 mmol, 1.49 equiv.), and trifluoromethanesulfonic anhydride (15.3 mL, 26.25 g, 93 mmol, 1.07 equiv.) were used. The target product, (2-(isopropoxyethyl)trifluoromethanesulfonyl)imide(**H[IESI]**), was obtained in 45.6 % isolated yield.

^{1}H NMR (DMSO-d$_6$, 400 MHz, δ in ppm): 9.49 (s, 1H, N-***H***), 3.62-3.53 (m, 1H, O-C***H***), 3.41 (t, $^{3}J_{H/H}$ = 11.0 Hz, 2H, C***H***$_2$-O), 3.26 (t, $^{3}J_{H/H}$ = 5.50 Hz, 2H, N-C***H***$_2$), 1.10(d, $^{3}J_{H/H}$ = 5.95 Hz, 6H, O-CH-(C***H***$_3$)$_2$). ^{13}C{^{1}H} NMR (DMSO-d$_6$, 101 MHz, δ in ppm): 123.36 (q, $^{1}J_{C/F}$ = 336.08 Hz, ***C***F$_3$), 70.96 (s, N- CH$_2$-***C***H$_2$), 70.48 (s, O-***C***H), 46.47 (s, N-***C***H$_2$), 22.65 (s, O-***C***H$_3$). ^{19}F NMR (DMSO-d$_6$, 471 MHz, δ in ppm): -75.80 (s, C***F***$_3$).

Li[IESI]:Lithium (2-isopropoxyethyl)trifluoromethanesulfonyl)imide)

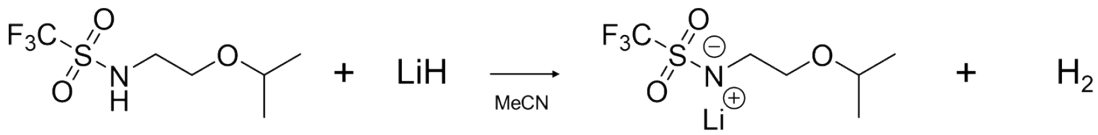

The same method used for synthesizing Li[TfN2O2O2] was applied to prepare Li[IESI]. Lithium hydride (0.12 g, 15 mmol, 1.36 equiv.) was reacted with (2-(isopropoxyethyl)trifluoromethanesulfonyl)imide(2.5 g, 11 mmol, 1.00 equiv.). The reaction yielded 1.86 g of Lithium (2-(isopropoxyethyl)trifluoromethanesulfonyl)imide(**Li[IESI]**) (7.7 mmol, 72.5 % isolated yield).

^{1}H NMR (DMSO-d$_6$, 600 MHz, δ in ppm): 3.49-3.40 (m, 1H, O-C***H***), 3.23 (t, $^{3}J_{H/H}$ = 15.11 Hz, 2H, C***H***$_2$-O), 2.94 (t, $^{3}J_{H/H}$ = 7.79 Hz, 2H, N-C***H***$_2$), 1.00 (d, $^{3}J_{H/H}$ = 5.95 Hz, 6H, O-CH-C***H***$_3$). ^{13}C{^{1}H} NMR (DMSO-d$_6$, 150 MHz, δ in ppm): 125.01 (q, $^{1}J_{C/F}$ = 332.84 Hz, ***C***F$_3$), 70.96 (s, N- CH$_2$-***C***H$_2$), 70.48 (s, O-***C***H), 46.47 (s, N-***C***H$_2$), 22.65 (s, O-***C***H$_3$). ^{19}F NMR (DMSO-d$_6$, 564 MHz, δ in ppm): -75.77 (s, C***F***$_3$).

H[ETFSI]: 2-(2-(2-methoxyethoxy)ethoxy)-N-((trifluoromethyl)sulfonyl)ethane-1-sulfonimide

The synthesis of H[ETFSI] was based on a previous report.[3]

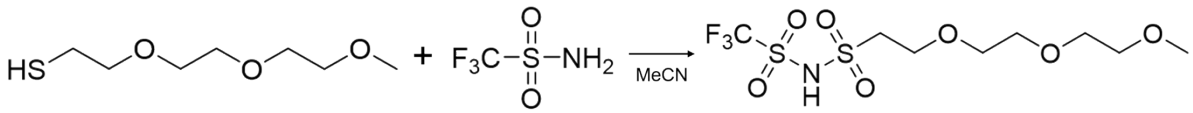

A mixture of 2-(2-(2-methoxyethoxy)ethoxy)ethane-1-thiol (2 mmol), 30% H_2O_2 (6 mmol, 0.6 mL) and $SOCl_2$ (2 mmol, 0.14 mL) was stirred in CH_3CN at 25 °C for an appropriate time. After completion of the reaction as indicated by TLC, a solution of amine (2 mmol) in pyridine (1 mL) was added to the reaction mixture. The resulting mixture was stirred at room temperature until TLC showed complete disappearance of starting material, then acidified with 2N HCl solution and extracted with EtOAc. The organic layer was washed with H_2O and brine and dried over $MgSO_4$. The filtrate was evaporated, and the corresponding pure sulfonimide was obtained as a crystalline solid. Recrystallization from a mixture of ethanol and water affords analytically pure product, **HETFSI**.

^{1}H NMR (MeOH-d_4, 500 MHz, δ in ppm): 8.96 (s, 1H, -N***H***), 3.89 (t, 1H, *J* = 5.5 Hz), 3.83 (t, 1H, $^3J_{H/H}$ = 5.0 Hz), 3.69 (t, 1H, $^3J_{H/H}$ = 5.5 Hz), 3.57-3.50 (m, 6H), 3.43 (t, 2H, $^3J_{H/H}$ = 5.0 Hz), 3.36 (t, 1H, $^3J_{H/H}$ = 6.0 Hz), 3.24 (s, 3H). ^{13}C{^{1}H} NMR (MeOH-d_4, 126 MHz, δ in ppm): 120.07 (q, $^1J_{C/F}$ = 321.55 Hz, CF_3), 71.80, 70.22, 69.58, 64.99, 61.66, 58.57, 36.17.

Li[ETFSI]: Lithium[2-(2-(2-methoxyethoxy)ethoxy)-N-((trifluoromethyl)sulfonyl)ethane-1-sulfonimide][4]

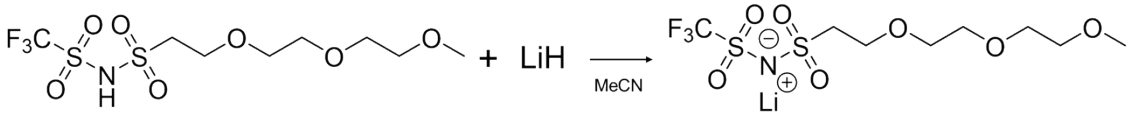

Lithium hydride (0.141 g, 18 mmol, 1.50 equiv.) was suspended in dry acetonitrile (50 mL) in a 100 mL Schlenk flask. HETFSI (11 mmol, 1.00 equiv.) was then added portionwise to the suspension in an ice bath under an argon atmosphere. After completion of the addition, the reaction mixture was stirred for 12 h. The resulting mixture was filtered through a filter cannula into a separate Schlenk flask. The solvent was removed under reduced pressure, and the crude product was recrystallized from acetone to afford a solid, which was dried under vacuum at 50 °C to give **LiETFSI** in 68% yield.

^{1}H NMR (MeOH-d_4, 500 MHz, δ in ppm): 3.74 (t, 2H, $^{3}J_{H/H}$ = 6.5 Hz), 3.57-3.62 (m, 6H), 3.52 (t, 2H, $^{3}J_{H/H}$ = 4.5 Hz), 3.34 (s, 3H), 2.49 (t, 2H, $^{3}J_{H/H}$ = 6.5 Hz). ^{13}C{^{1}H} NMR (MeOH-d_4, 126 MHz, δ in ppm): 71.83, 70.07, 70.04, 70.00, 65.64, 62.01, 57.76. ^{19}F NMR (MeOH-d_4, 471 MHz, δ in ppm): −79.70 (s, CF_3).

Force Field parameters

Table S1 Force field parameters used for MD simulations (Atom types were explained in **(Figure S1**).

Nonbonding parameters

atom	σ (Å)	ε (kcal mol^{-1})	α (a.u.)
NIE	3.55	0.170	7.4
SO	3.55	0.250	16.0
OS	3.00	0.130	5.0
FC	3.15	0.053	2.5
CF	3.50	0.066	8.0
CS	3.50	0.066	8.0
CT	3.50	0.066	8.0
OG	3.10	0.140	4.0
HC	2.50	0.030	1.0
Li	2.48	0.003	0.0

$E_{\text{nonbond}} = 4\varepsilon\,[(\sigma/r)^{12} - (\sigma/r)^{6}]$

Bond stretching parameters

bond	k_s (kcal mol^{-1} Å^{-2})	r_0 (Å)
NIE-SO	744.0	1.546
SO-OS	1274.0	1.450
SO-CF	471.0	1.835
CF-FC	884.0	1.340
NIE-CS	268.0	1.454
CS-CS	268.0	1.529
CS-CT	268.0	1.529
CS-OG	570.0	1.408
CT-OG	570.0	1.408
CS-HC	340.0	1.090
CT-HC	340.0	1.090

$E_{str} = k_s (r - r_0)^2$

Angle bending parameters

angle	k_θ (kcal mol^{-1} rad^{-2})	θ_0 (deg)
SO-NIE-CS	80.0	112.0
NIE-SO-CF	195.0	105.2
NIE-SO-OS	189.0	118.0
OS-SO-CF	208.0	102.6
SO-CF-FC	116.0	110.4
FC-CF-FC	187.0	108.6
NIE-CS-CS	58.35	107.7
NIE-CS-HC	37.5	110.7
CS-CS-CS	58.35	112.7
CS-CS-HC	37.5	110.7
CS-CT-HC	37.5	110.7
CT-CS-HC	37.5	110.7
HC-CS-HC	33.0	107.8
HC-CT-HC	33.0	107.8
CS-CS-OG	80.0	109.0
CT-CS-OG	80.0	109.0
HC-CS-OG	35.0	109.0
HC-CT-OG	35.0	109.0
CS-OG-CS	55.0	106.8
CS-OG-CT	55.0	106.8

$E_{bend} = k_\theta(\theta - \theta_0)^2$

Torsional parameters

dihedral	V_1 (kcal mol^{-1})	V_2 (kcal mol^{-1})	V_3 (kcal mol^{-1})
NIE-SO-CF-FC	0.0	0.0	0.3
OS-SO-CF-FC	0.0	0.0	0.171

CF-SO-NIE-CS	-0.4	3.7	0.0
OS-SO-NIE-CS	0.0	0.0	0.0
SO-NIE-CS-CS	-8.0	-1.5	0.0
SO-NIE-CS-HC	0.0	0.0	0.0
NIE-CS-CS-CS	0.85	0.2	0.2
NIE-CS-CS-HC	0.0	0.0	0.0
NIE-CS-CS-OG	4.3	4.0	0.202
CS-CS-CS-OG	0.85	0.2	0.2
OG-CS-CS-OG	4.3	4.0	0.202
OG-CS-CS-HC	0.0	0.0	0.0
OG-CS-CT-HC	0.0	0.0	0.0
CS-CS-OG-CS	-0.98	-0.97	0.25
CT-CS-OG-CS	-0.98	-0.97	0.25
CS-CS-OG-CT	-1.9	-0.97	0.25
HC-CS-OG-CS	0.0	0.0	0.67
HC-CS-OG-CT	0.0	0.0	0.67
HC-CT-OG-CS	0.0	0.0	0.67

$E_{\text{torsion}} = \Sigma\ V_n/2\ (1 + \cos(n\varphi))$

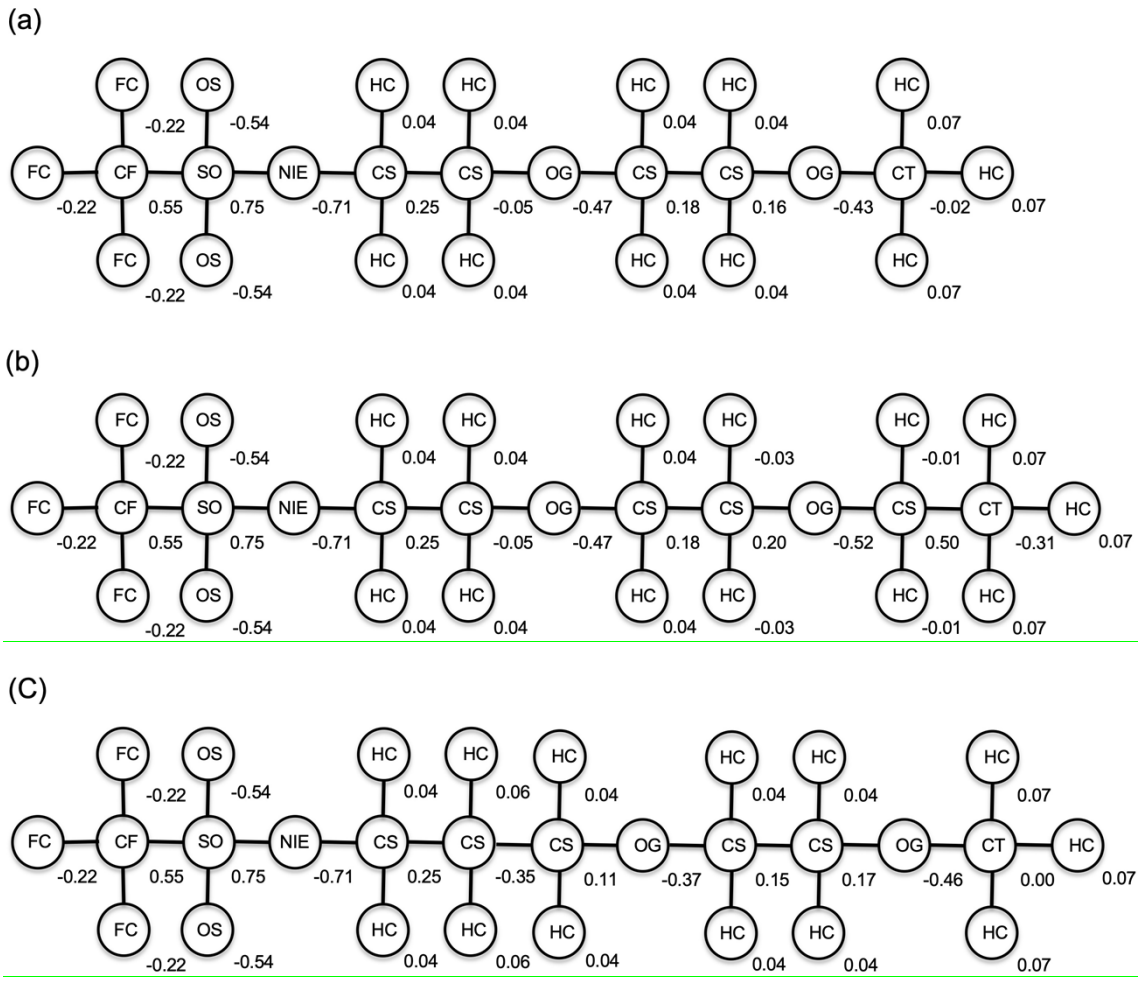

Figure S1 Atom types and atomic charges used for MD simulations: (a) $[TfN2O2O1]^-$ anion; (b) $[TfN2O2O2]^-$ anion; (c) $[TfN3O2O1]^-$ anion.

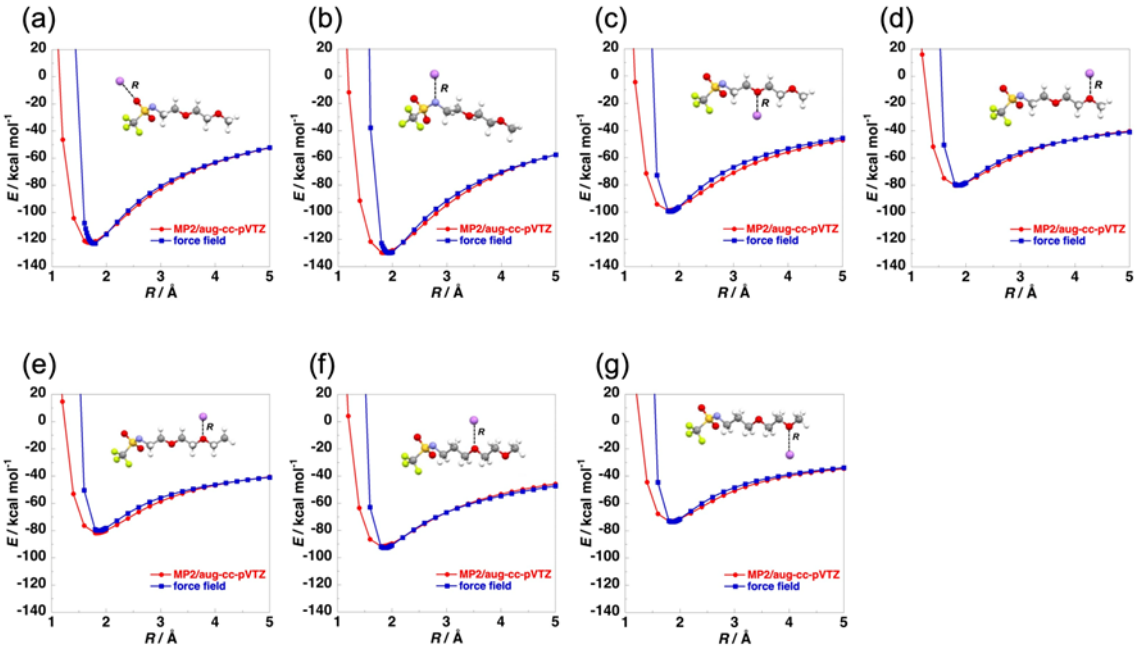

Figure S2 Comparison of interaction energy potentials of Li^+ with anions obtained by MP2/aug-cc-pVTZ level *ab initio* and force field calculations with changing Li…O or Li…N distances (*R*): (a) Li^+ is located on the extension of the S-O bond; (b) Li^+ is located on the bisector of the S-N-C angle: (c-g) Li^+ is located on the bisector of the C-O-C angle.

Solvent property

Table S2. Relative permittivity of solvent and solubility of each Li salt.[5]

	polarity								
	Hexane	Toluene	DCM	Acetone	Acetonitrile	Ethanol	Methanol	DMSO	H_2O
Relative permittivity (ε_r)	1.88	2.38	8.93	20.56	35.94	24.55	32.66	46.45	78.36
Li[TfN5]	×	×	×	○	○	○	○	○	○
Li[TfN7]	×	×	×	○	○	○	○	○	○
Li[TfN2O2]	×	×	×	○	△	○	○	○	○
Li[TfN3O1]	×	×	×	○	△	○	○	○	○
Li[TfN2O2O1]	×	△	○	○	○	○	○	○	○
Li[TfN3O2O1]	×	△	○	○	○	○	○	○	○
Li[TfN2O2O2]	×	△	○	○	○	○	○	○	○
Li[MMP]	×	×	×	○	△	○	○	○	○
Li[IESI]	×	×	×	○	△	○	○	○	○
Li[ETFSI]	×	×	×	×	○	○	○	○	○

Substances that are miscible are denoted by ○, those that are miscible only in small amounts by △, and those that are essentially immiscible by ×.

Lithium Transference Number for DCM-based electrolytes

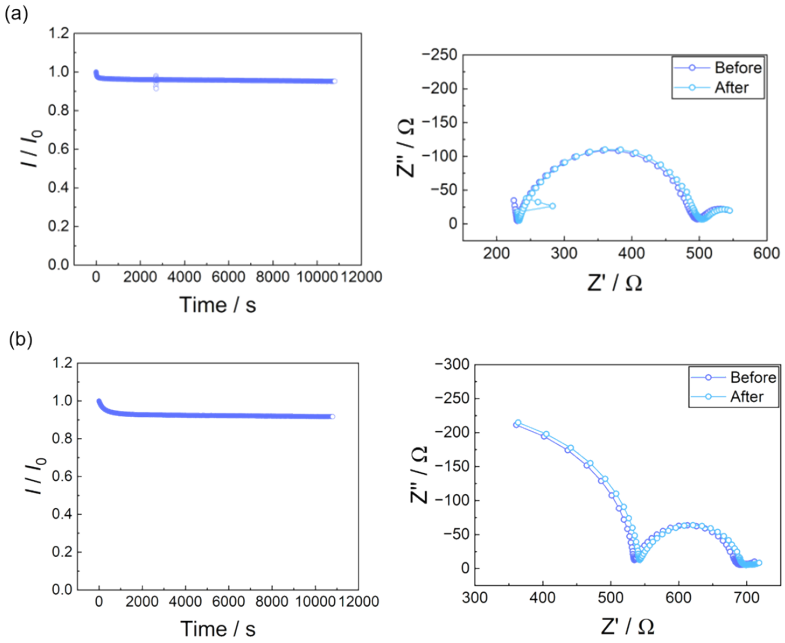

Figure S3. The potentiostatic polarization curves and Nyquist plots before and after the potentiostatic polarization of Li/Li symmetric cells using DCM-based electrolytes, (a) 1 M [Li(DCM)][TfN2O2O1] and 3 M [Li(DCM)][TfN2O2O1] at 30 °C.

Thermal properties

Table S3. Decomposition temperatures of the Li salts.

Li salt	T_d / °C
Li[TfN5]	236.5
Li[TfN7]	245.4
Li[TfN2O2]	289.2
Li[TfN3O1]	269.0
Li[TfN2O2O1]	251.9
Li[TfN2O2O2]	248.9
Li[TfN3O2O1]	257.0
Li[MMP]	289.7
Li[IESI]	293.2
Li[ETFSI]	291.0

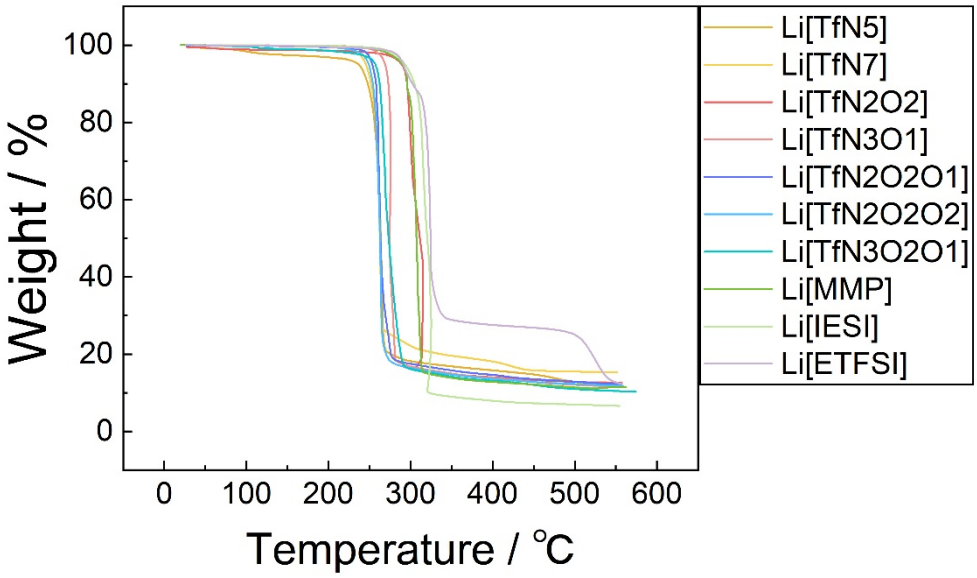

Figure S4. TGA curves of synthesized Li salts.

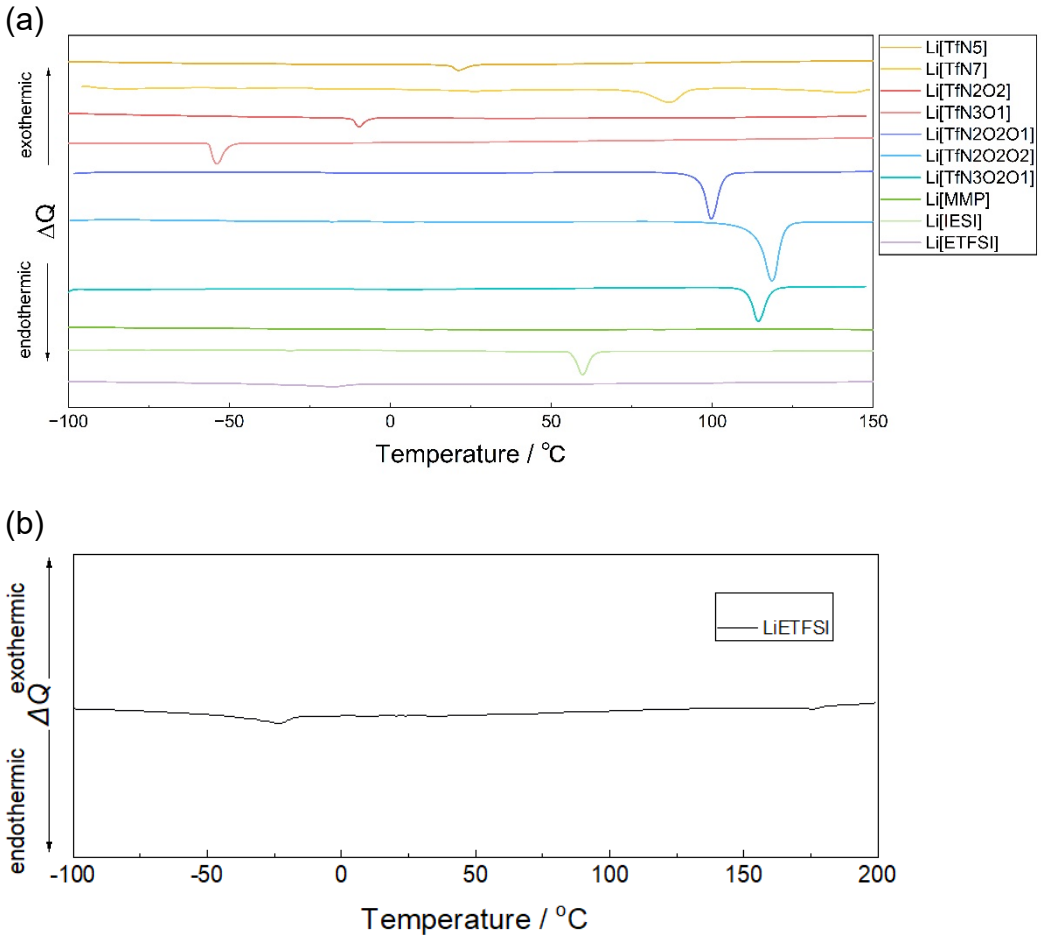

Figure S5. (a) DSC results of all synthesized Li salts. (b) An extended DSC of Li[ETFSI] with the investigated temperature range of −100 to 200 °C.

Quantum chemical calculations

Ab initio and DFT calculations were performed using Gaussian 16.[2] Basis set superposition error (BSSE)[6] was corrected for all intermolecular interaction energy (E_{int}) calculations using the counterpoise method.[7] The stabilization energy due to complex formation from isolated species (E_{form}) was calculated as the sum of E_{int} and deformation energy (E_{def}), which is the increase in energy of the anion due to the deformation of geometry associated with complex formation.[8] Torsional angle was fixed and other internal geometrical parameters were optimized in the calculations of torsional potentials. The optimized geometries of isolated molecules at the MP2/6-311G** level were used for the calculations of intermolecular interaction energy potentials without further geometry optimizations.

MD simulation

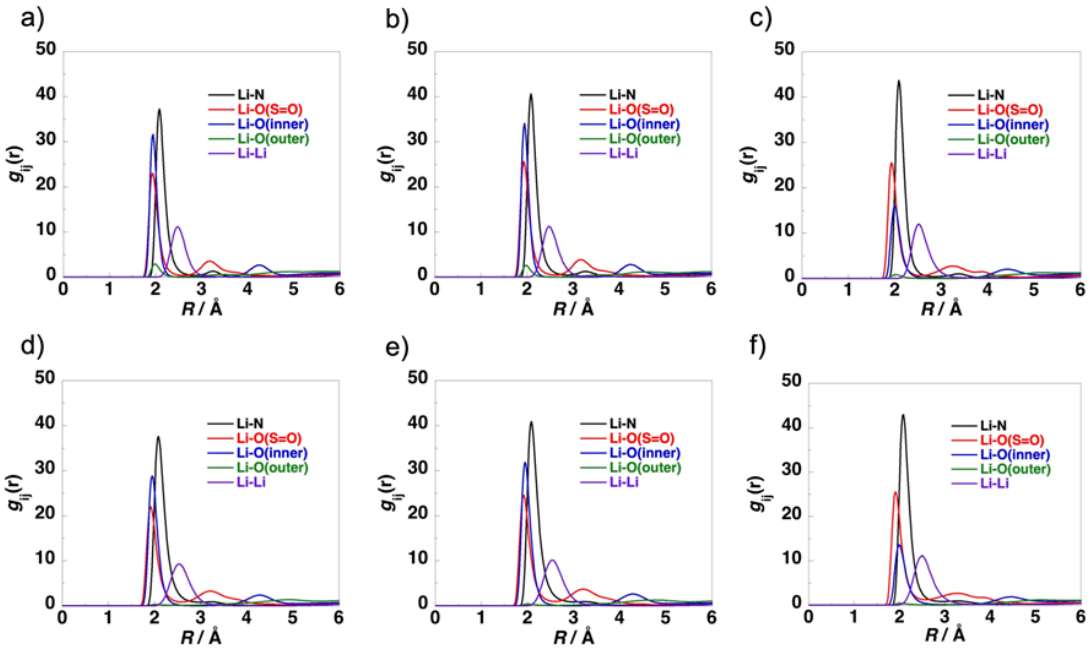

Figure S6. (a) Site-site intermolecular radial distribution functions calculated for Li[TfN2O2O1], Li[TfN2O2O2] and Li[TfN3O2O1]: (a-c) at 413.15 K; (d-f) 613.15 K; (a, d) Li[TfN2O2O1]; (b, e) Li[TfN2O2O2]; (c, f) Li[TfN3O2O1].

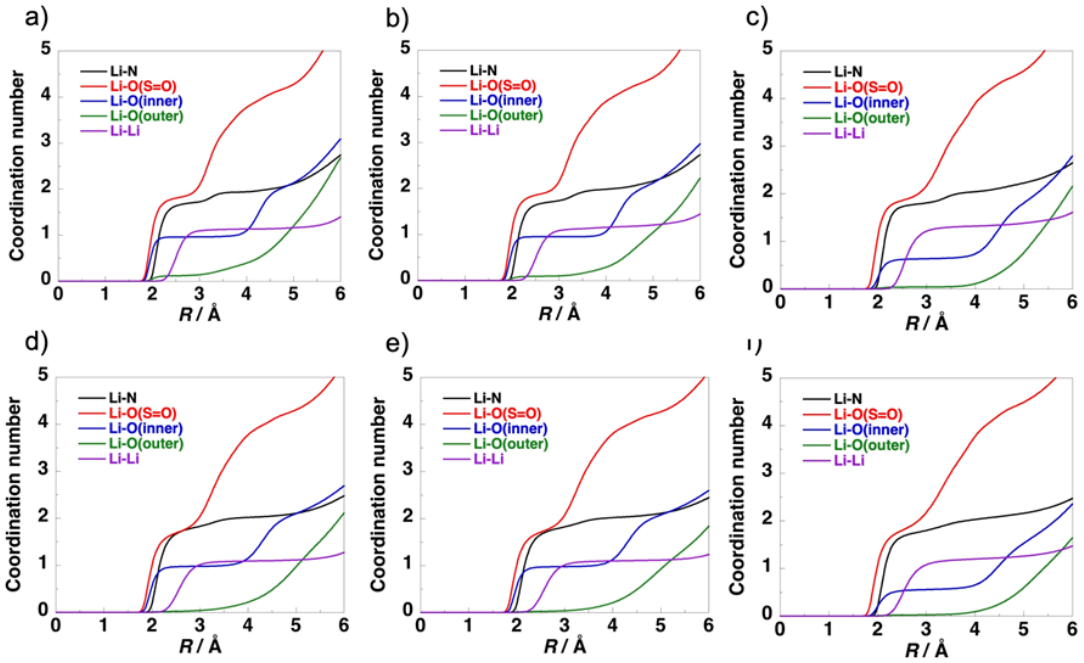

Figure S7. Cumulative coordination numbers around Li^+ ions calculated for Li[TfN2O2O1], Li[TfN2O2O2] and Li[TfN3O2O1]: (a-c) at 413.15 K; (d-f) 613.15 K; (a, d) Li[TfN2O2O1]; (b, e) Li[TfN2O2O2]; (c, f) Li[TfN3O2O1].

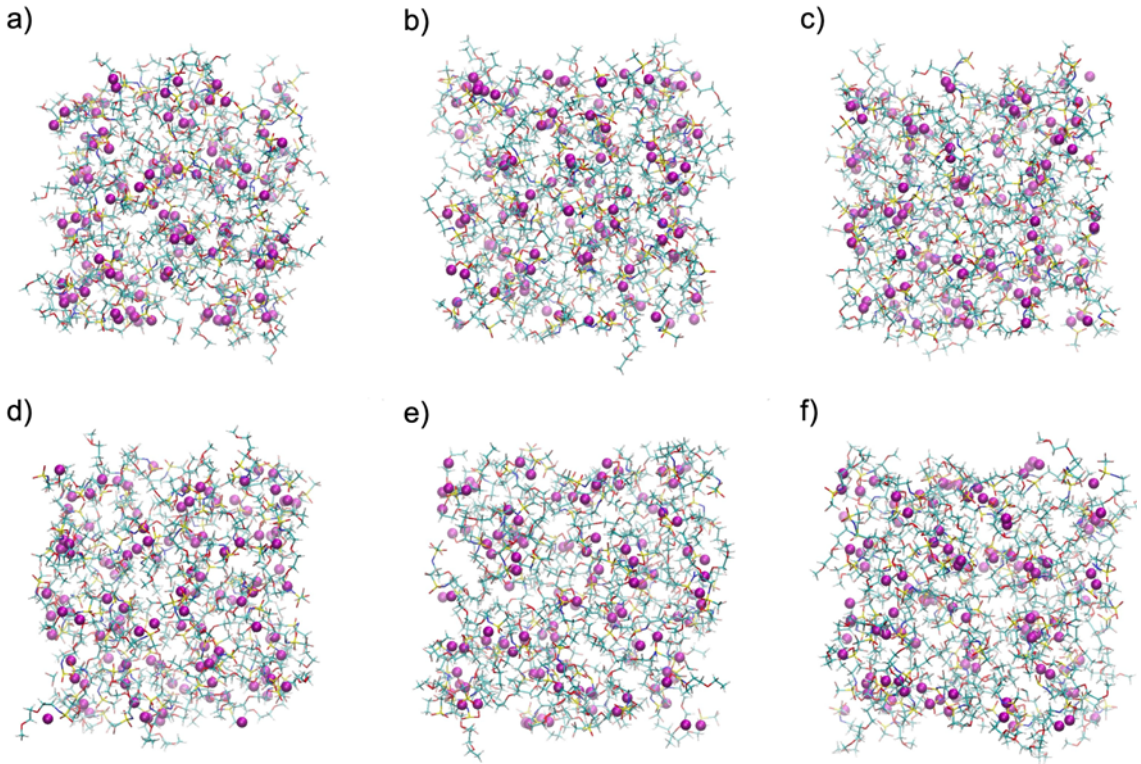

Figure S8. Snapshots of Li[TfN2O2O1], Li[TfN2O2O2] and Li[TfN3O2O1]. Carbon, hydrogen, oxygen, nitrogen, fluorine, sulfur, and lithium atoms are shown in light blue, white, red, blue, pink, yellow, and purple, respectively. Li^+ ions are represented using a space-filling model, whereas other atoms are shown using a wireframe model: (a-c) at 413.15 K; (d-f) 613.15 K; (a, d) Li[TfN2O2O1]; (b, e) Li[TfN2O2O2]; (c, f) Li[TfN3O2O1].

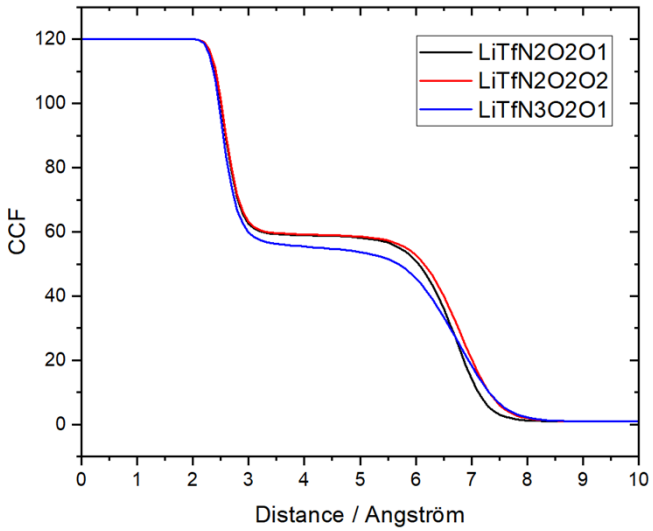

Figure S9. Li-Li cluster distance distribution function for Li[TfN2O2O1], Li[TfN2O2O2], and Li[TfN3O2O1] at 613.15 K.

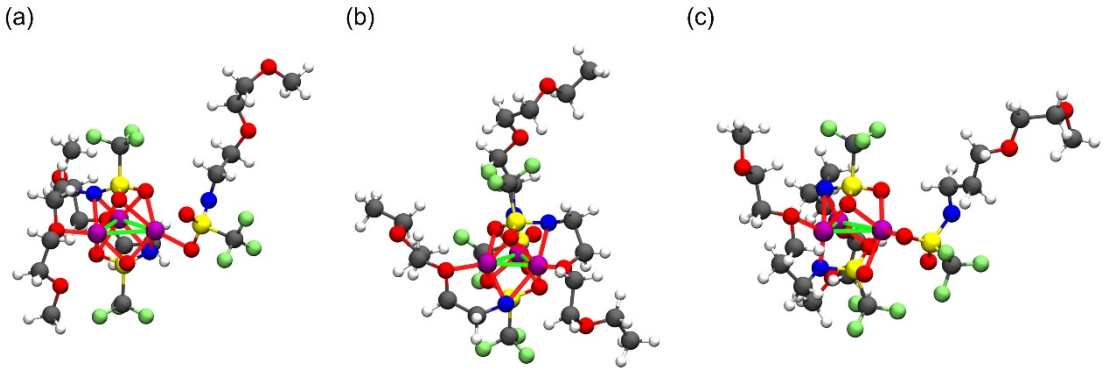

Figure S10. Snapshots of representative trimers in (a) Li[TfN2O2O1], (b) Li[TfN2O2O2] and (c) Li[TfN3O2O1] at 613.15K.

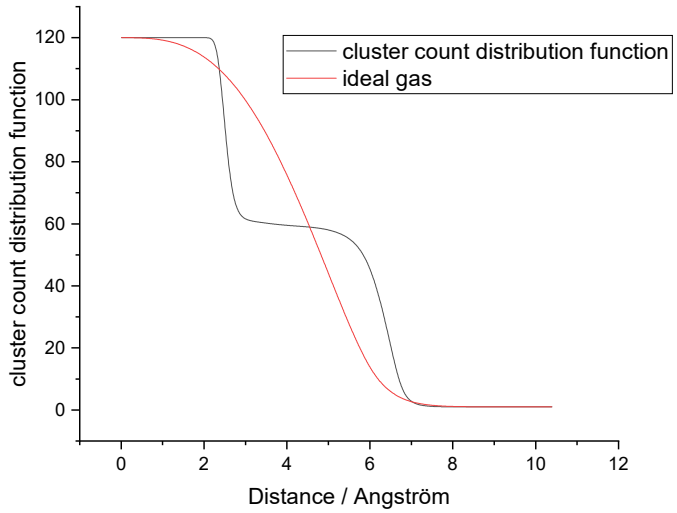

Figure S11. Li-Li cluster distance distribution function for Li[TfN2O2O1] at 413 K (ideal gas for comparison).

Table S4. Cluster statistics at 4.0 Å cutoff at 413 K for Li[TfN2O2O1].

members	Fraction of Li atoms
1	8.6%
2	65%
3	23%
4	3.4%
5	<0.1%

Analysis of interactions in the $Li_2[TfN2O2O1]_2$ complex

Intermolecular interactions in the $Li_2[TfN2O2O1]_2$ complex were analyzed to elucidate the origin of its stability. The optimized geometry of the complex, calculated at the B3LYP/6-311G** level with Grimme's D3 dispersion correction, is shown in **Figure S12**. A geometry obtained from a snapshot of the MD simulation was used as the initial structure. Vibrational analysis confirms that the optimized structure is an energy minimum.

Interaction energies between ions in the complex were calculated at the same level, with incorporating BSSE correction by the counterpoise method. The results are summarized in **Table S5**. Although strong repulsion exists between anions and between cations, there is significant attraction between anions and cations. The anion-anion (E_{AB}) and cation-cation (E_{CD}) interactions are 68.66 and 88.94 kcal mol^{-1}, respectively. The cation-anion interactions (E_{AC}, E_{AD}, E_{BC}, and E_{BD}) range from –134.65 to –178.15 kcal mol^{-1}. The total cation-anion attraction ($E_{cation\text{-}anion}$= –632.32 kcal mol^{-1}) significantly outweighs the total repulsion from anion-anion and cation-cation interactions ($E_{anion\text{-}anion}$ + $E_{cation\text{-}cation}$ = 157.60 kcal mol^{-1}). This strong attraction is the primary origin of stability of the complex. The total interaction energy for the complex (E_{ABCD}) is –412.82 kcal mol^{-1}, while the sum of 2-body interactions ($E_{2\text{-}body}$) is –474.72 kcal mol^{-1}. Thus, the many body interaction ($E_{many} = E_{ABCD} - E_{2\text{-}body}$) contributes repulsively by 61.90 kcal mol^{-1}.

Table S5. Interaction energy between ions in the $Li_2[TfN2O2O1]_2$ complex. Geometry of $Li_2[TfN2O2O1]_2$ complex is shown in Figure S12.

	Interaction energy[a]
$E_{AB} = E_{anion\text{-}anion}$ (anion-anion)	68.66
E_{AC} (anion-cation)	–142.37
E_{AD} (anion-cation)	–178.15
E_{BC} (anion-cation)	–177.15
E_{BD} (anion-cation)	–134.65
$E_{CD} = E_{cation\text{-}cation}$ (cation-cation)	88.94
$E_{anion\text{-}anion} + E_{cation\text{-}cation} = E_{AB} + E_{CD}$[b]	157.60
$E_{cation\text{-}anion} = E_{AC} + E_{AD} + E_{BC} + E_{BD}$[c]	–632.32
$E_{2\text{-}body} = E_{anion\text{-}anion} + E_{cation\text{-}cation} + E_{cation\text{-}anion}$[d]	–474.72
E_{ABCD}[e]	–412.82
$E_{many} = E_{ABCD} - E_{2\text{-}body}$[f]	61.90

[a] Interaction energy in kcal/mol.

[b] Sum of interaction energy between anions and that between cations.

[c] Sum of interaction energies between anions and cations.

[d] Total 2-body interaction energy.

[e] Interaction energy for $Li_2[TfN_2O_2O_1]_2$ complex.

[f] Many body interactions.

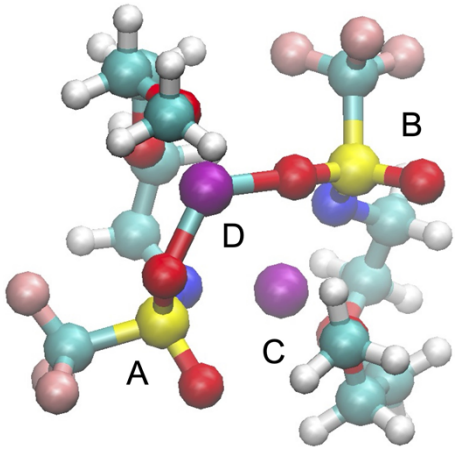

Figure S12. Optimized structure of $Li_2[TfN2O2O1]_2$ complex at the B3LYP/6-311G** + D3 level. Carbon, hydrogen, oxygen, nitrogen, fluorine, sulfur, and lithium atoms are shown in light blue, white, red, blue, pink, yellow, and purple, respectively.

Voronoi-based local structure analysis

To gain deeper insight into the molten-state structure of the ether-functionalized lithium salts, a Voronoi-based local structure analysis was performed. Unlike ensemble-averaged methods, Voronoi tessellation captures local coordination environments by identifying atoms in the immediate vicinity of a target species, enabling a more detailed assessment of ion-ion correlations and clustering behavior. As shown in **Figure S13**, the Voronoi neighborhood analysis reveals a substantial population of clusters and aggregates, consistent with the trends inferred from RDF and Li-Li clustering analyses.

For example, for Li[TfN2O2O1] at 413 K (**Figure S13a**), analysis of the local environment around Li1 shows that carbon atoms along the ether chain (C2-C4) appear with high probability, whereas the occurrence probability decreases toward the chain terminus (C5 and C6). A similar trend is observed for oxygen atoms: the sulfonyl oxygens (O1 and O2) and the inner ether oxygen (O3) are frequently located near Li^+, while the terminal ether oxygen (O4) exhibits a significantly lower probability (≈ 0.40). These results indicate that the ether-chain terminus (C6 and O4) interacts weakly with Li^+ and behaves as a relatively "free" moiety in the molten state, consistent with the weak terminal-oxygen coordination inferred from the RDF analysis.

A comparable spatial differentiation is observed within the TfN moiety. While the sulfonyl group and imide nitrogen (S1, O1/O2, and N1) are found in close proximity to Li^+ with near-unity probability, the CF_3 group (C1 and F1/F2/F3) exhibits a markedly lower neighbor probability.

Although nanoscale segregation was previously described in terms of "ionic" TfN/Li^+ domains and "non-ionic" ether-chain domains, the present Voronoi analysis clarified a more nuanced segregation pattern. Specifically, the ionic region comprises Li^+ together with the sulfonyl unit and adjacent mid-chain segment (up to C4), whereas the non-ionic region consists of the CF_3 group and the ether-chain terminus (C5, O4, and C6). This interpretation is further supported by the high probability of adjacency between the ether-terminal carbon (C6) and the fluorine atoms (F1/F2/F3) of the CF_3 group. Collectively, these results indicate that such spatially resolved ionic/non-ionic nanoscale segregation plays a key role in governing the molten-state structure and characteristic physicochemical properties.

Importantly, the overall spatial differentiation revealed by the Voronoi analysis is preserved at 613.15 K, indicating that the local coordination motif and ionic/non-ionic segregation are largely insensitive to temperature within the investigated range (**Figure S13b**). A similar local structural pattern is also observed for Li[TfN2O2O2] and Li[TfN3O2O1], where Li^+ preferentially resides near the sulfonyl and inner ether oxygen atoms, while the terminal ether groups and CF_3 moieties remain weakly associated (**Figure S13c, d**). These results confirm that the characteristic nanoscale segregation and cluster-based coordination motif are common structural features across this series of ether-functionalized asymmetric lithium salts.

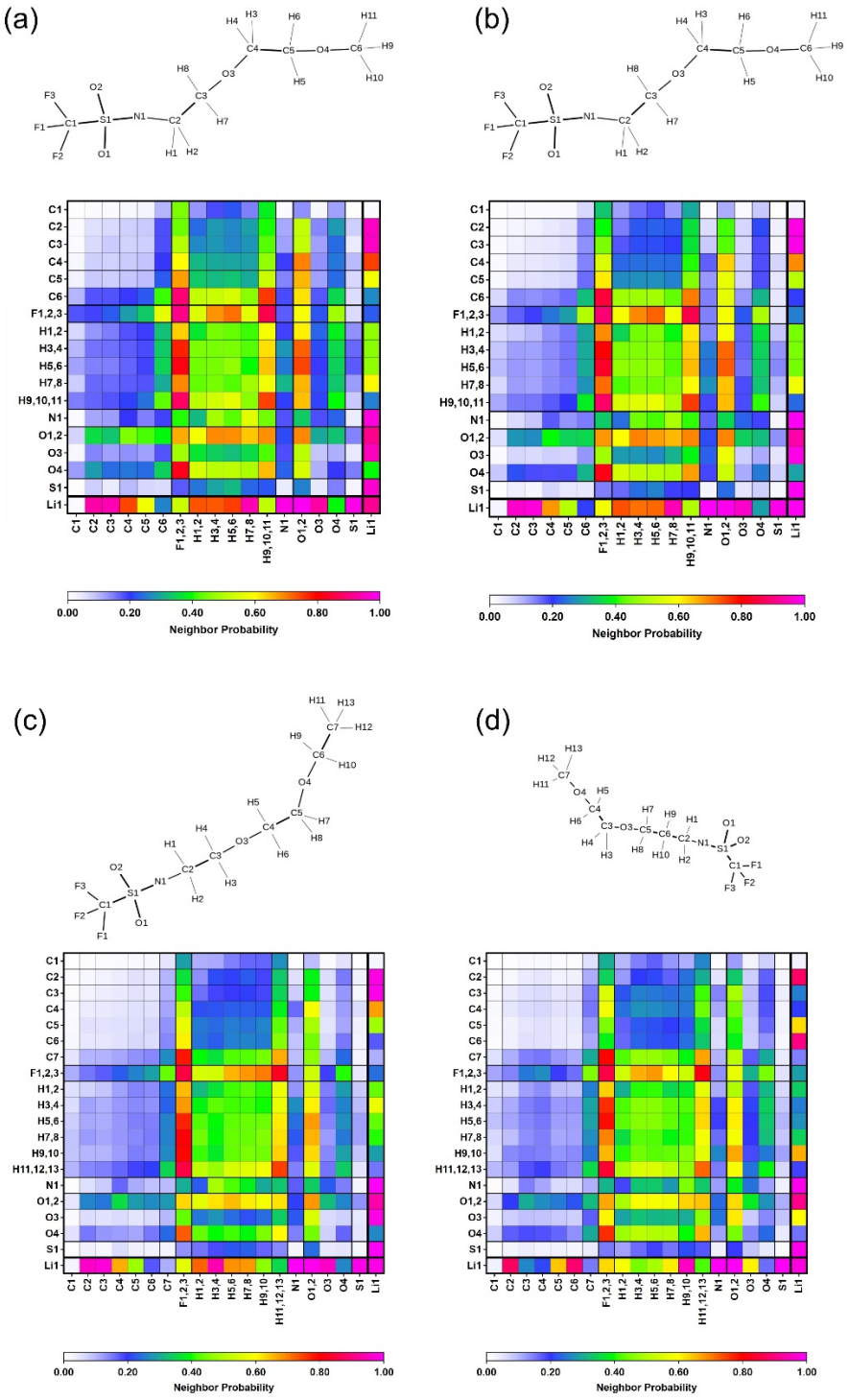

Figure S13. Voronoi neighborhood analysis for (a) Li[TfN2O2O1] at 413.15 K, (b) Li[TfN2O2O1] at 613.15 K, (c) Li[TfN2O2O2] at 613.15 K, and (d) Li[TfN3O2O1] at 613.15 K.

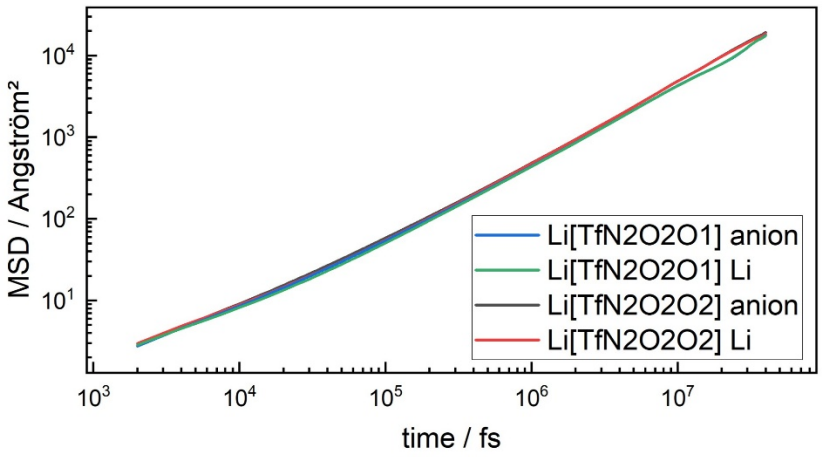

Figure S14. MSD of Li^+ ions and anions in Li[TfN2O2O1] and Li[TfN2O2O2] at 613.15 K.

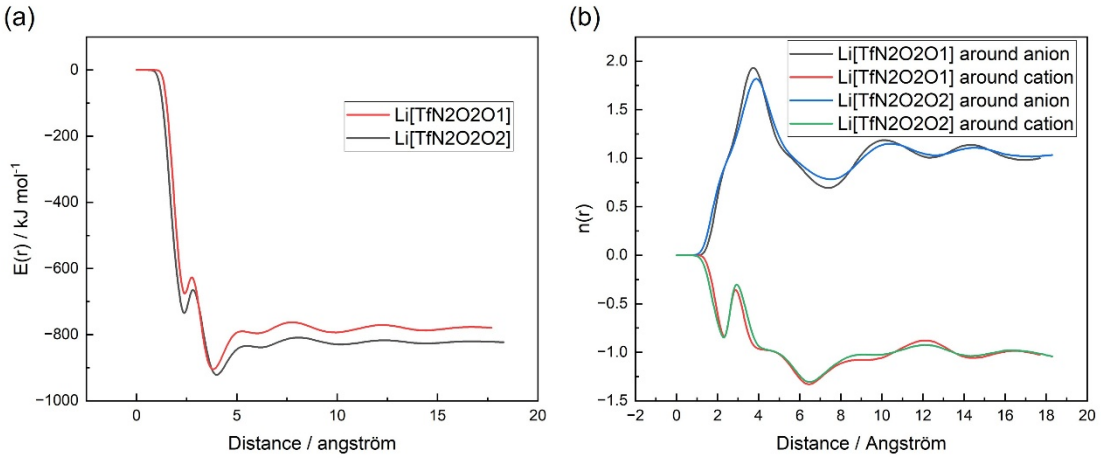

Figure S15. (a) Running integral of the Coulomb interaction energy calculated using integer charges on the center of mass, and (b) charge-weighted number integral of all counterions surrounding a central reference ion. For complete electrostatic screening, this function converges to +1 around an anion and to −1 around a cation.

Transport properties

Table S6. Self-diffusion coefficients of the lithium salts in their molten state, as determined by PFG-NMR.

sample	ion	Temp. / °C	D / 10^{-7} cm^2 s^{-1}	Log(D)
Li[TfN2O2O1]	Li^+	120	0.103	−0.986
		140	0.280	−0.553
	$[TfN2O2O1]^-$	120	0.106	−0.974
		140	0.274	−0.562
Li[TfN3O2O1]	Li^+	140	0.353	−0.452
	$[TfN3O2O1]^-$	140	0.387	−0.412
Li[TfN2O2O2]	Li^+	100	0.0393	−1.41
		120	0.133	−0.876
		140	0.377	−0.424
	$[TfN2O2O2]^-$	100	0.0389	−1.41
		120	0.135	−0.870
		140	0.341	−0.467
Li[FTA]	Li^+	100	0.0242	−1.62
		120	0.0620	−1.21
		140	0.151	−0.821
	$[FTA]^-$	120	0.0289	−1.54
		140	0.0745	−1.13

Table S7. Calculated densities and self-diffusion coefficients of ions

	T[a]	ρ[b]	D[c]	
			Li	Anion
Li[TfN2O2O1]	393.15	1.36	0.12	0.14
	413.15	1.35	0.34	0.40
	613.15	1.16	76	76
Li[TfN2O2O2]	393.15	1.31	0.22	0.24
	413.15	1.30	0.63	0.70
	613.15	1.10	74	74
Li[TfN3O2O1]	393.15	1.32	0.16	0.18
	413.15	1.31	0.53	0.60
	613.15	1.12	73	74

[a] Temperature in K.

[b] Density in g cm^{-3}.

[c] Self-diffusion coefficient in 10^{-7} cm^2 s^{-1}.

Table S8. Ionic conductivity of Li[TfN2O2O2] measured in the temperature range from 140 °C to 30 °C.

	T / °C	σ / S cm^{-1}	logσ
Li[TfN2O2O2]	140	4.85×10^{-5}	−4.31
	130	3.29×10^{-5}	−4.48
	120	2.12×10^{-5}	−4.67
	110	1.28×10^{-5}	−4.89
	100	7.23×10^{-6}	−5.14
	90	3.79×10^{-6}	−5.42
	80	1.83×10^{-6}	−5.74
	70	7.78×10^{-7}	−6.11
	60	2.90×10^{-7}	−6.54
	50	9.13×10^{-8}	−7.04
	40	2.41×10^{-8}	−7.62
	30	7.05×10^{-9}	−8.15

Lithium Transference Number

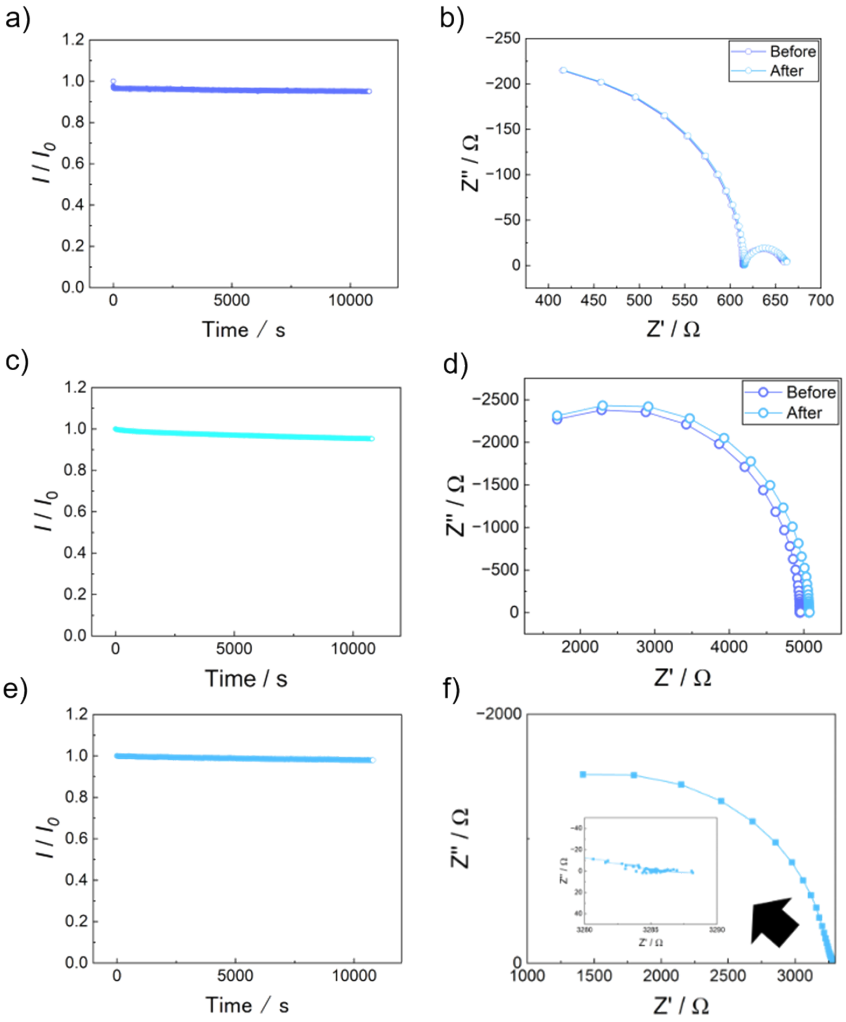

Figure S16. (a) The potentiostatic polarization curves, (b)Nyquist plots before and after the potentiostatic polarization of Li/Li symmetric cells using Li[TfN2O2O1] at 120 °C, (c) the potentiostatic polarization curves and (d) Nyquist plots of Li/Li symmetric cells using Li[TfN2O2O2] at 130 °C (e) the potentiostatic polarization curves and (f) Nyquist plots of Li/Li symmetric cells using Li[TfN3O2O1] at 130 °C.

Electrochemical properties

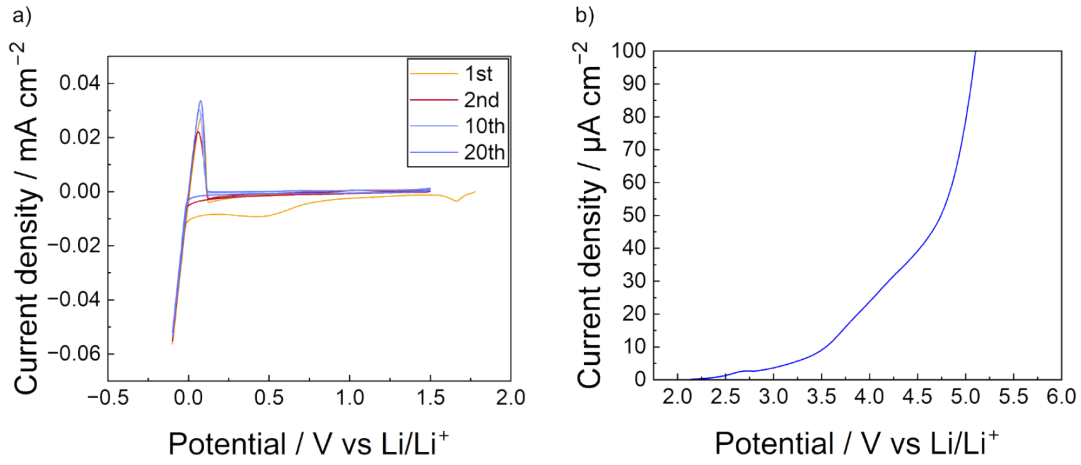

Figure S17. (a) Cyclic voltammograms on a Cu electrode at scan rate 1 mV s^{-1} and (b) linear sweep voltammograms on a SUS electrode of Li[TfN2O2O2] at 130 ℃.

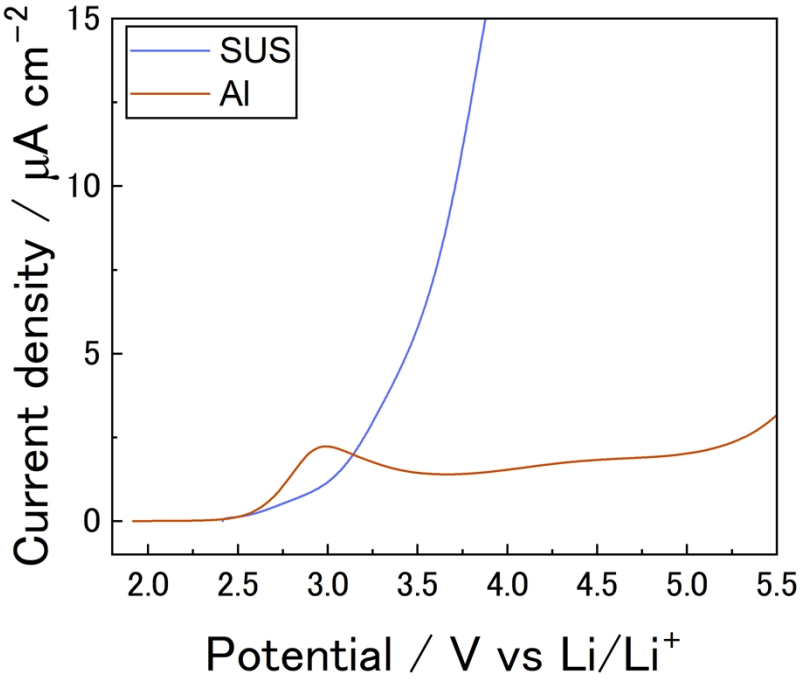

Figure S18. LSV curves in Li[TfN2O2O1] measured with different working electrodes at 130 °C.

Exchange current density

In this analysis, IR compensation was not applied. Instead, an apparent exchange current density, $j_{0,app}$, was evaluated from the linear low-overpotential approximation of the j–E response using the reverse scan, where E' denotes the potential referenced such that $E'(j = 0) = 0$.

Table S9. Exchange current density, as determined by cyclic voltammogram.

	$j_{0,app}$ / mA cm^{-2}			
	Li[TfN2O2O1]	Li[TfN2O2O2]	Li[TfN3O2O1]	Li[FTA]
±10 mV	0.0228	0.0163	0.0224	0.0516
±15 mV	0.0248	0.0167	0.0233	0.0531
±20 mV	0.0240	0.0170	0.0237	0.0555

NMR Spectra

H[TfN2O2O2]

^{1}H NMR

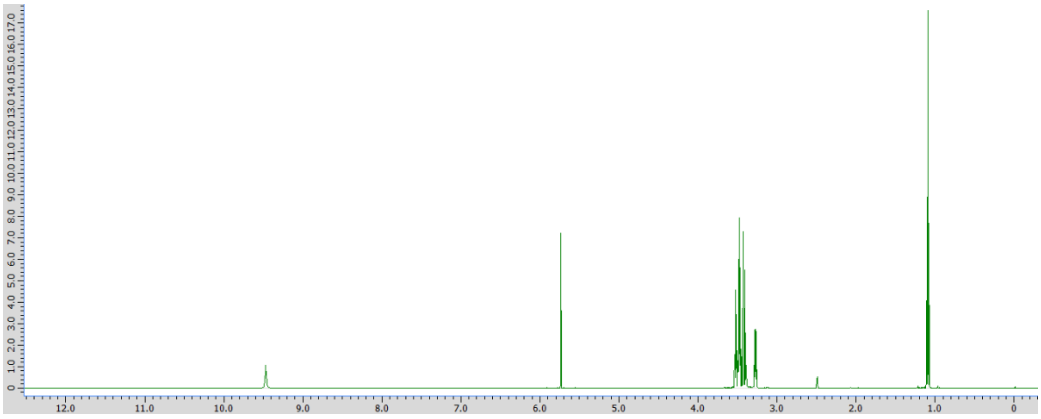

^{13}C NMR

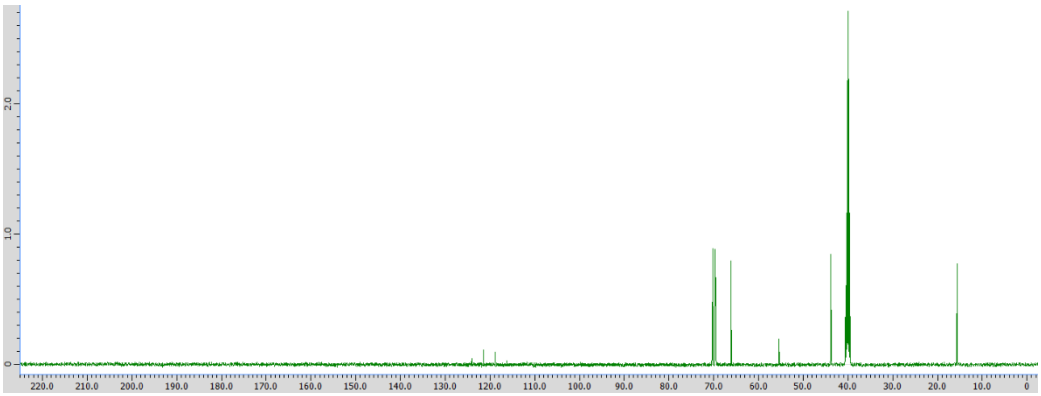

^{19}F NMR

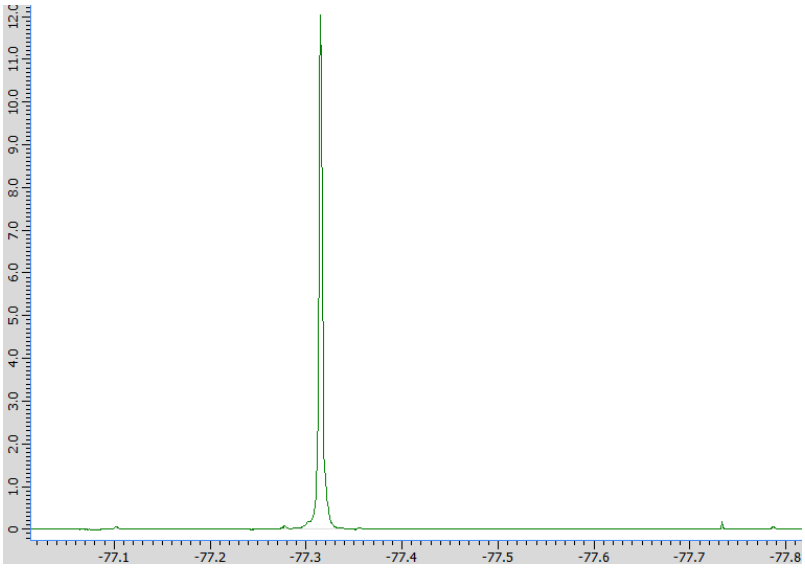

Li[TfN2O2O2]

^{1}H NMR

^{13}C NMR

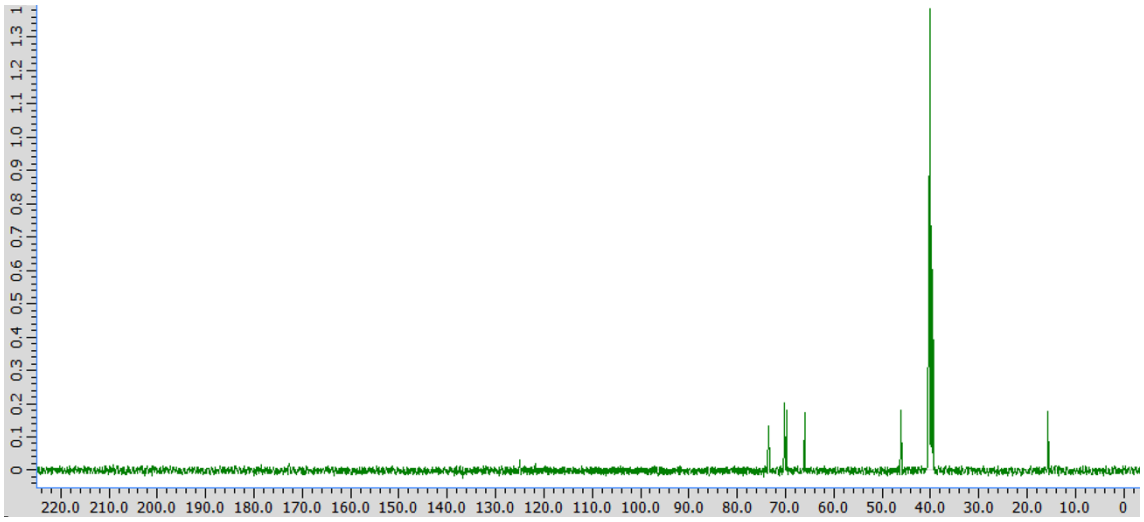

^{19}F NMR

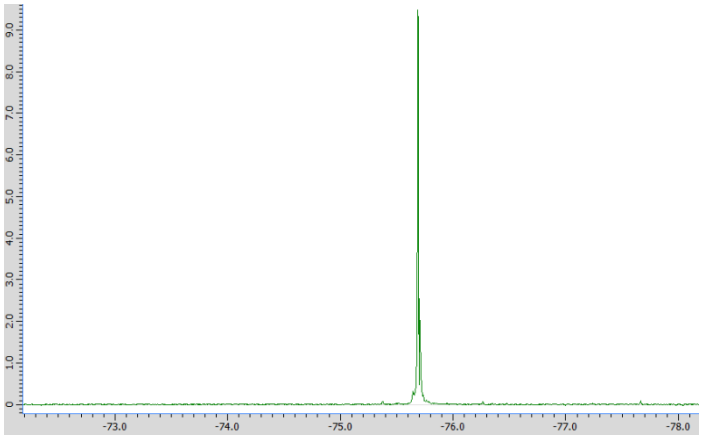

ESI-MS

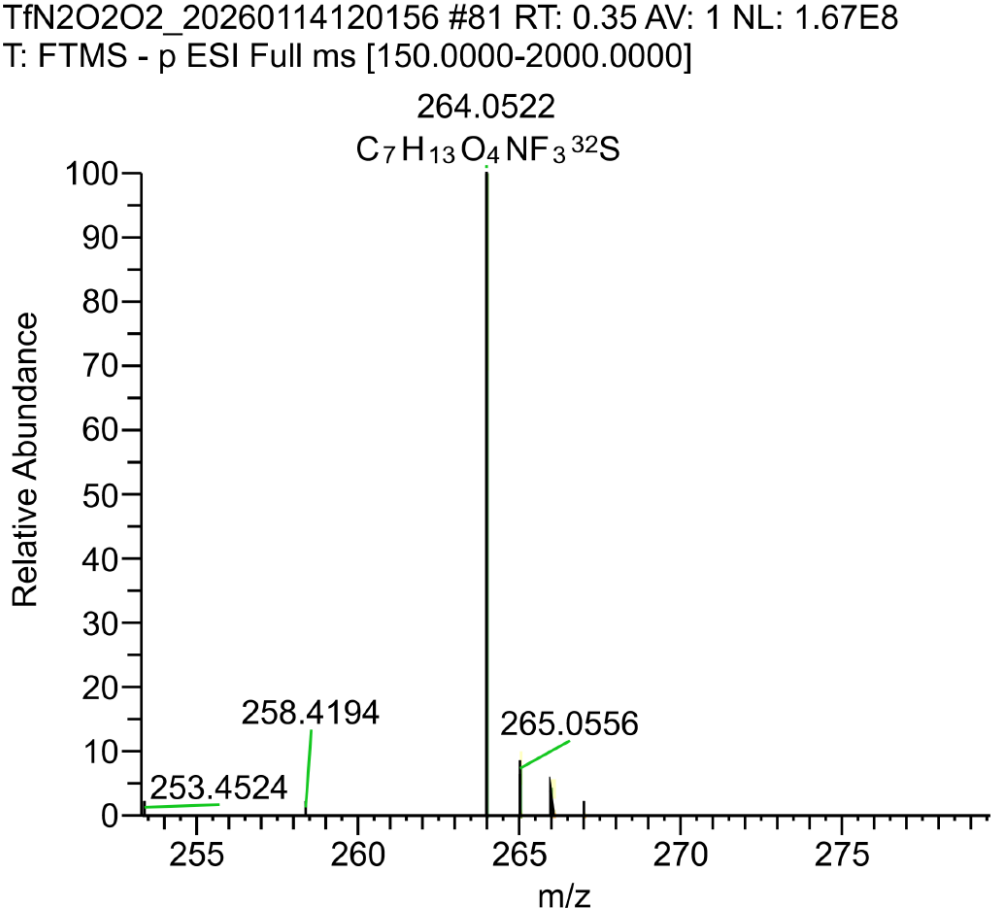
TfN2O2O2_20260114120156 #81 RT: 0.35 AV: 1 NL: 1.67E8
T: FTMS - p ESI Full ms [150.0000-2000.0000]
264.0522
C7H13O4NF332S
Relative Abundance
m/z
258.4194
265.0556
253.4524

H[TfN7]

^{1}H NMR

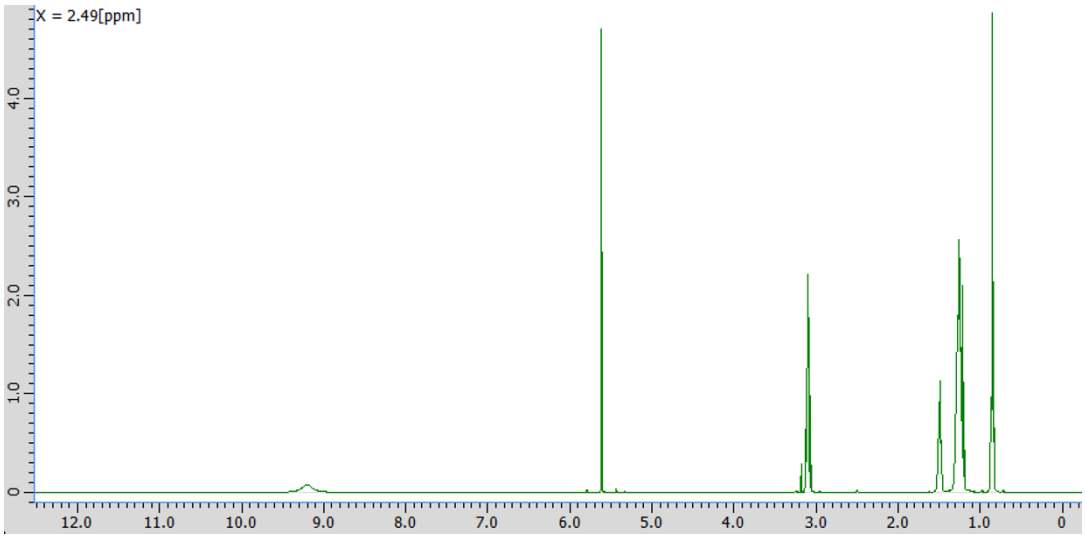

^{13}C NMR

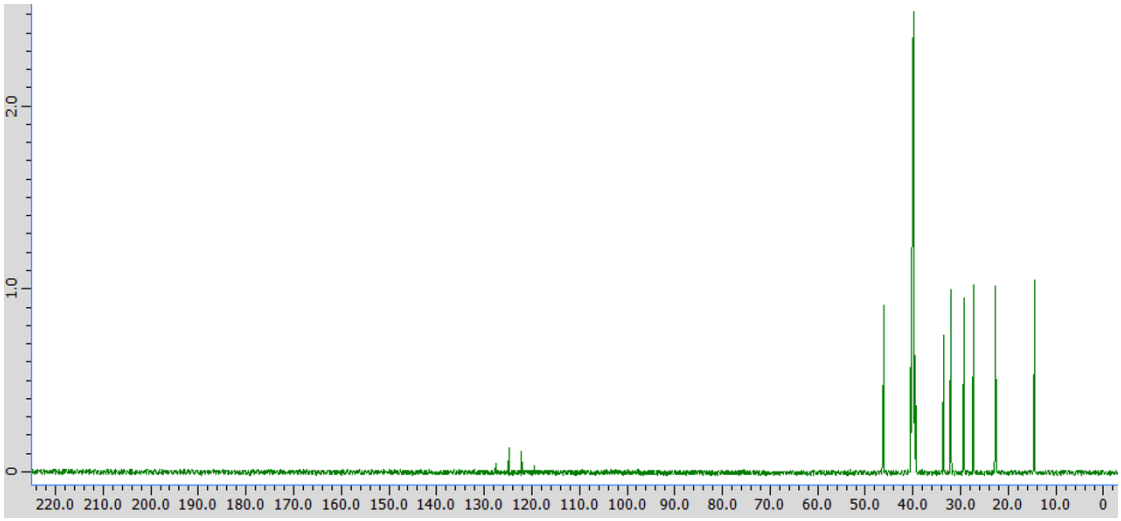

^{19}F NMR

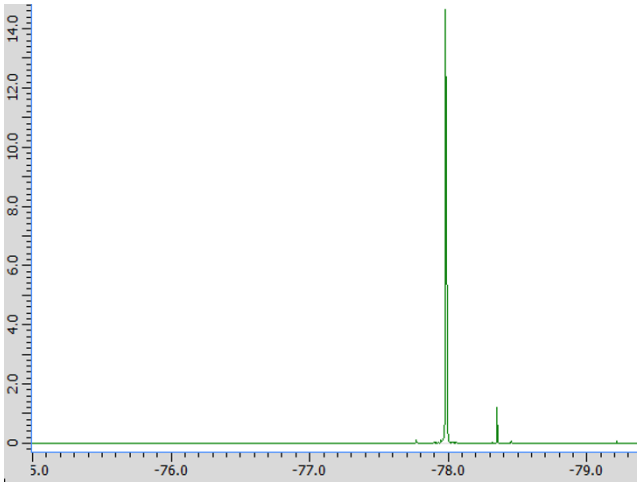

Li[TfN7]

^{1}H NMR

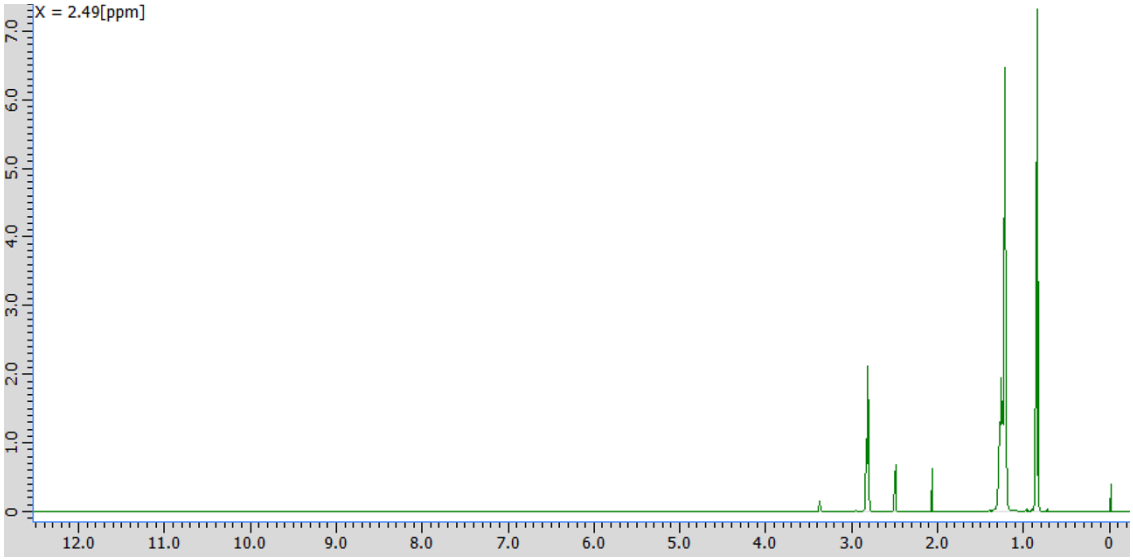

^{13}C NMR

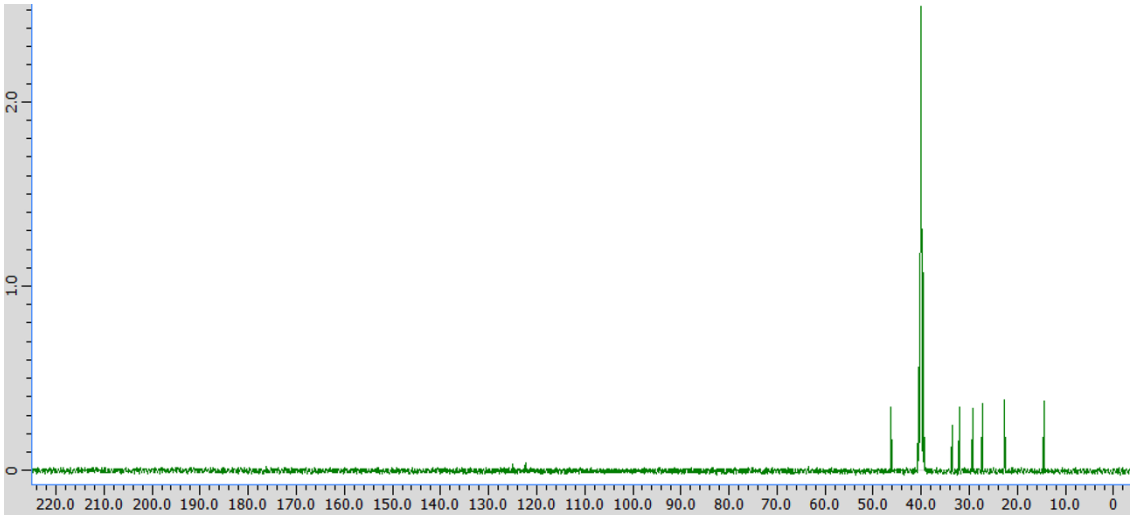

^{19}F NMR

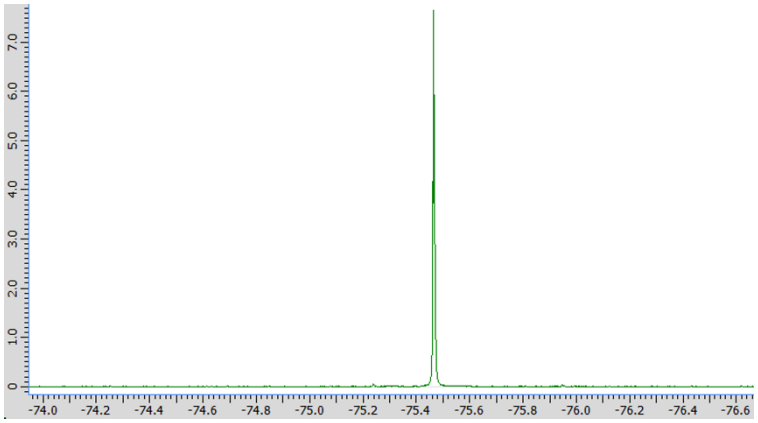
7.0
6.0
5.0
4.0
3.0
2.0
1.0
0
-74.0
-74.2
-74.4
-74.6
-74.8
-75.0
-75.2
-75.4
-75.6
-75.8
-76.0
-76.2
-76.4
-76.6

H[TfN2O2]

^{1}H NMR

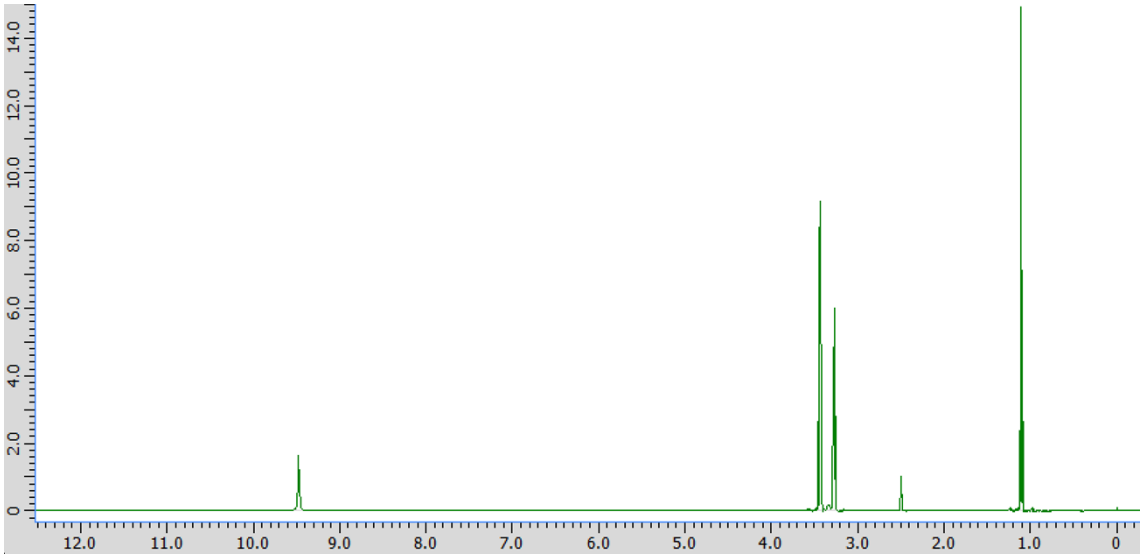

^{13}C NMR

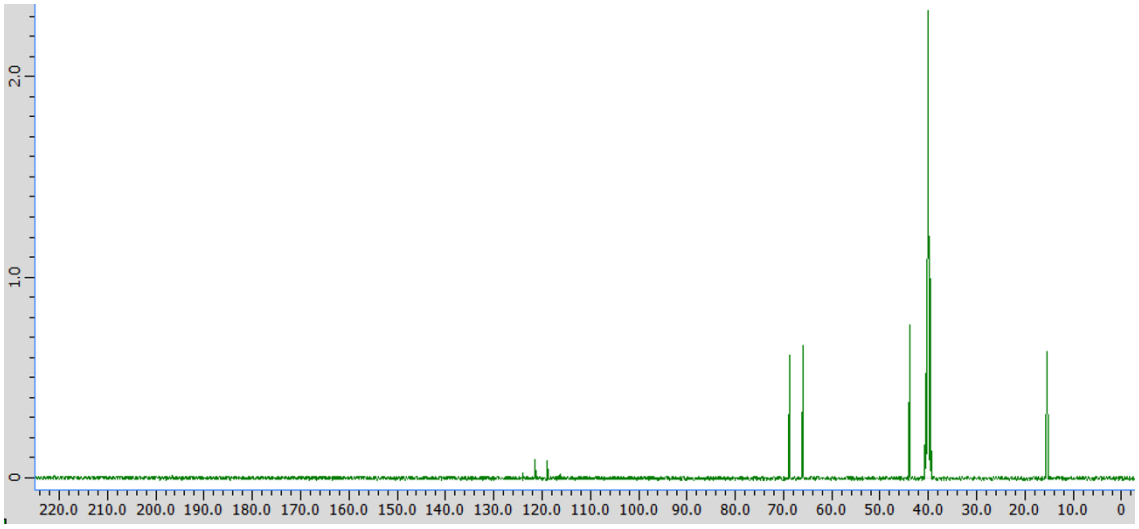

^{19}F NMR

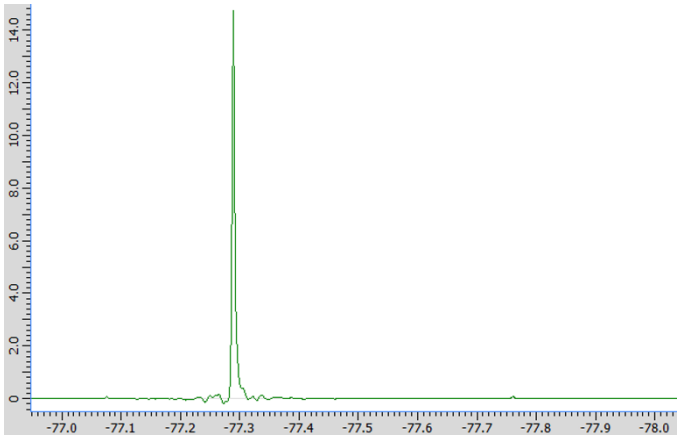

Li[TfN2O2]

^{1}H NMR

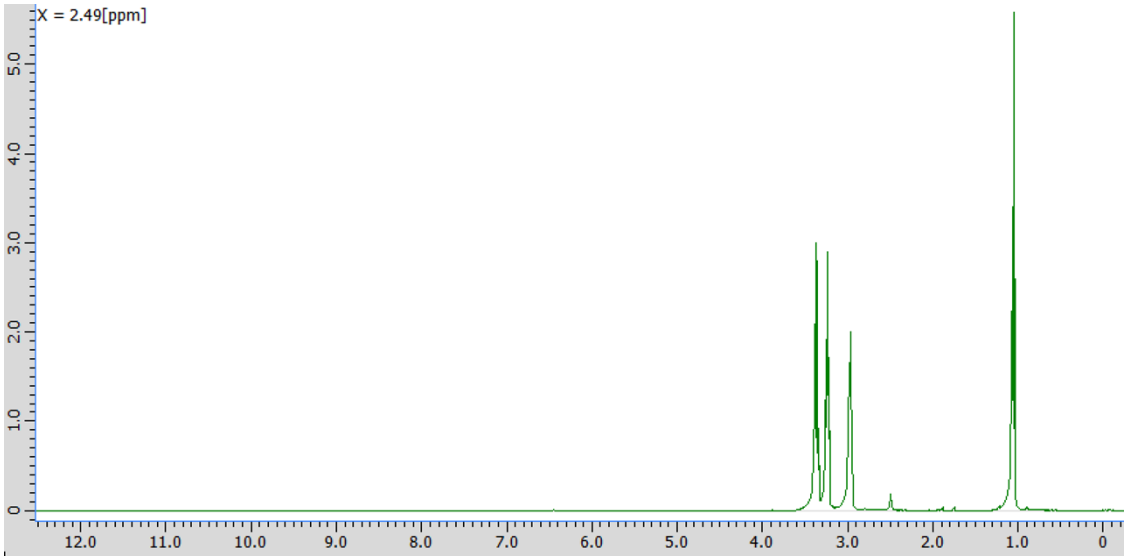

^{13}C NMR

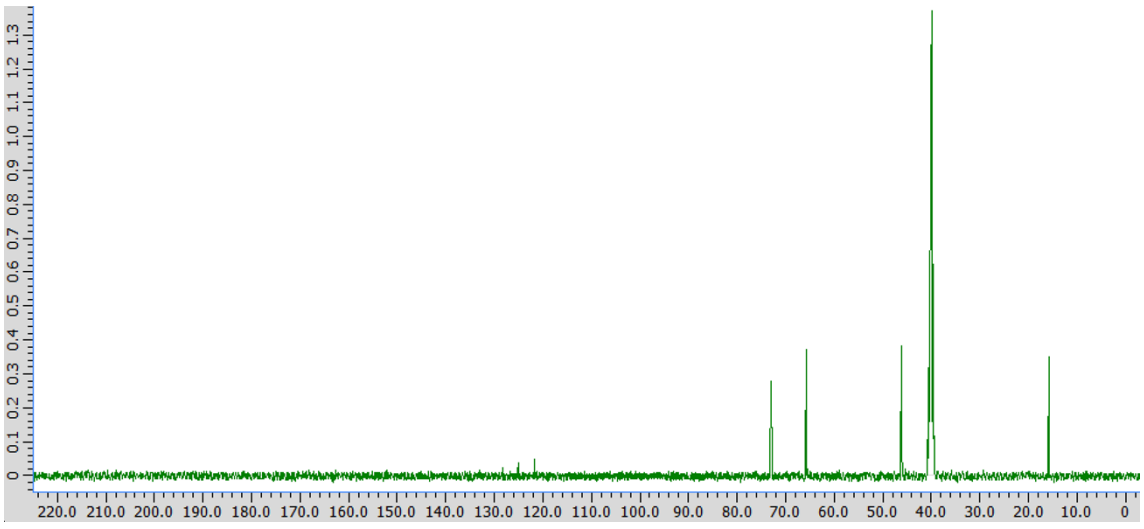

^{19}F NMR

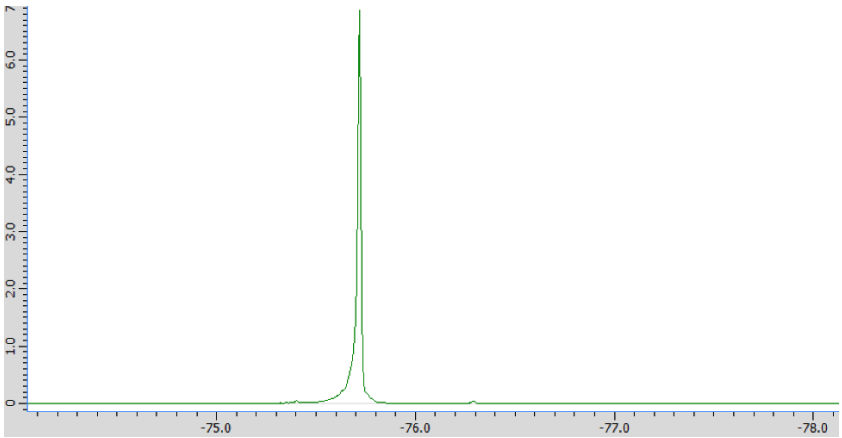

H[MMP]

^{1}H NMR

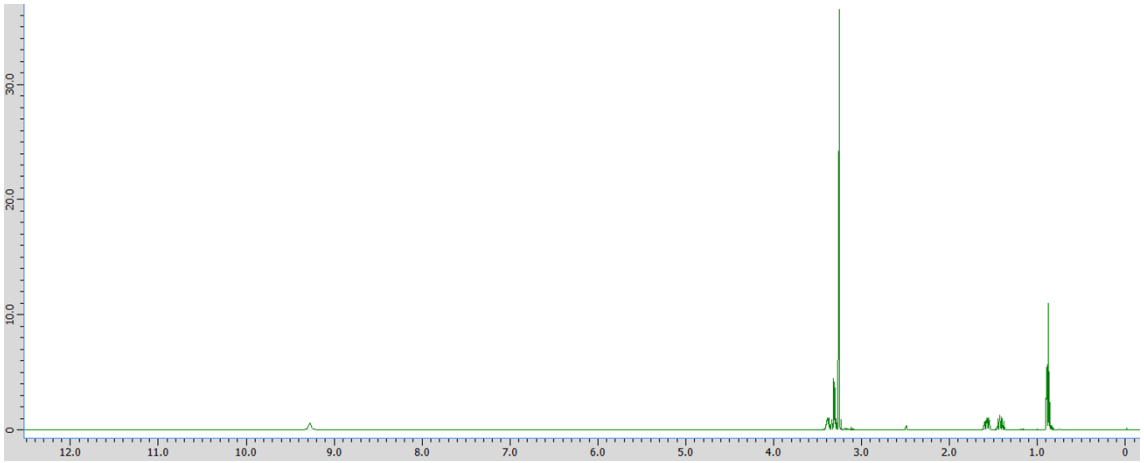

^{13}C NMR

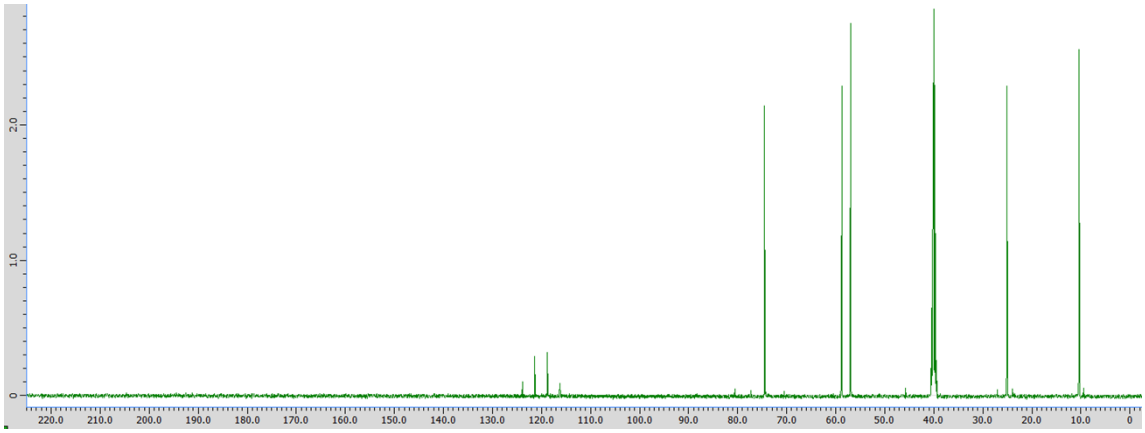

^{19}F NMR

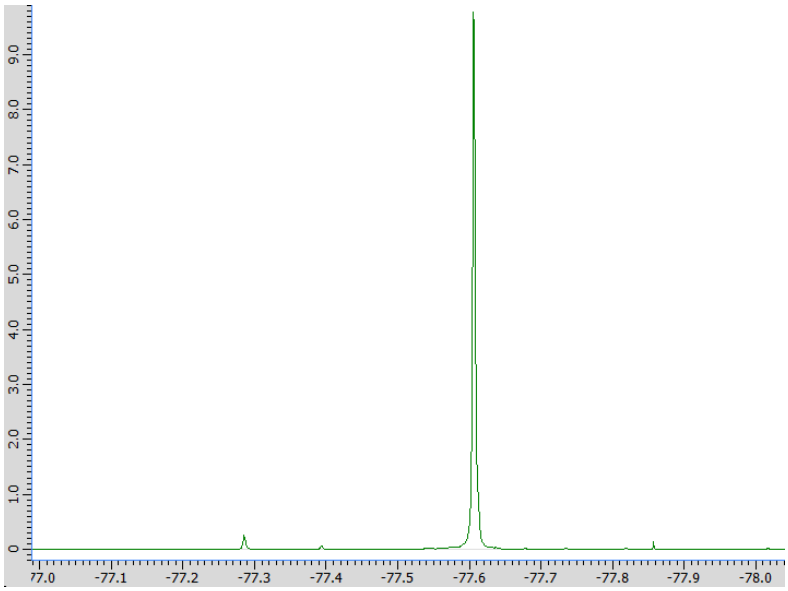

Li[MMP]

^{1}H NMR

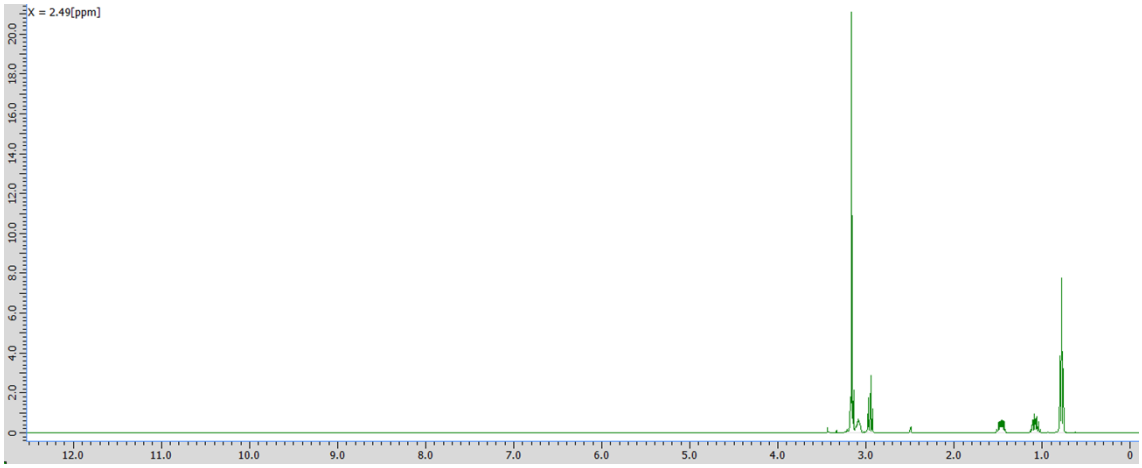

^{13}C NMR

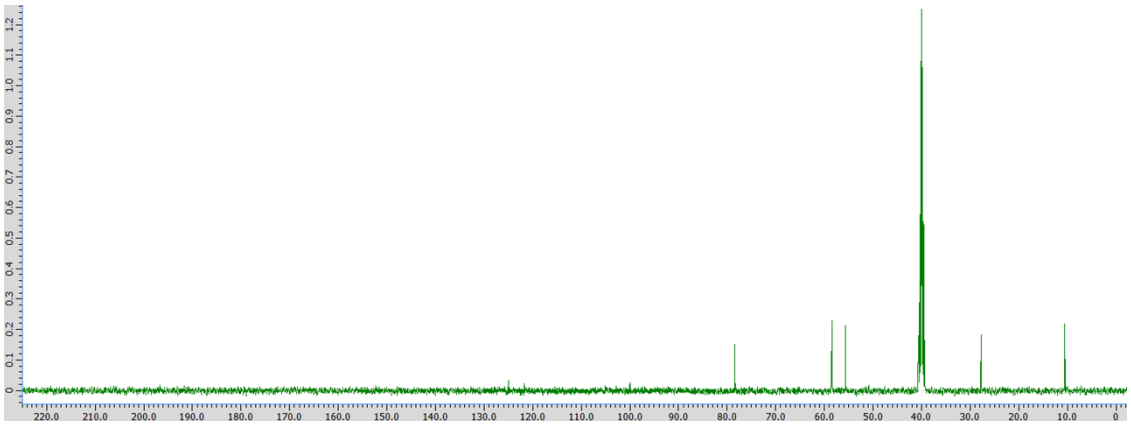

^{19}F NMR

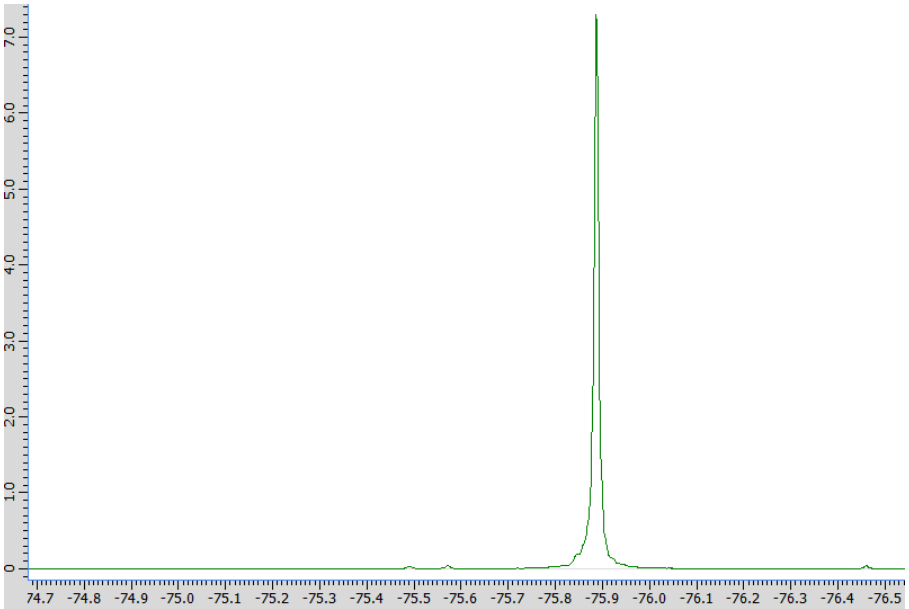

H[IESI]

^{1}H NMR

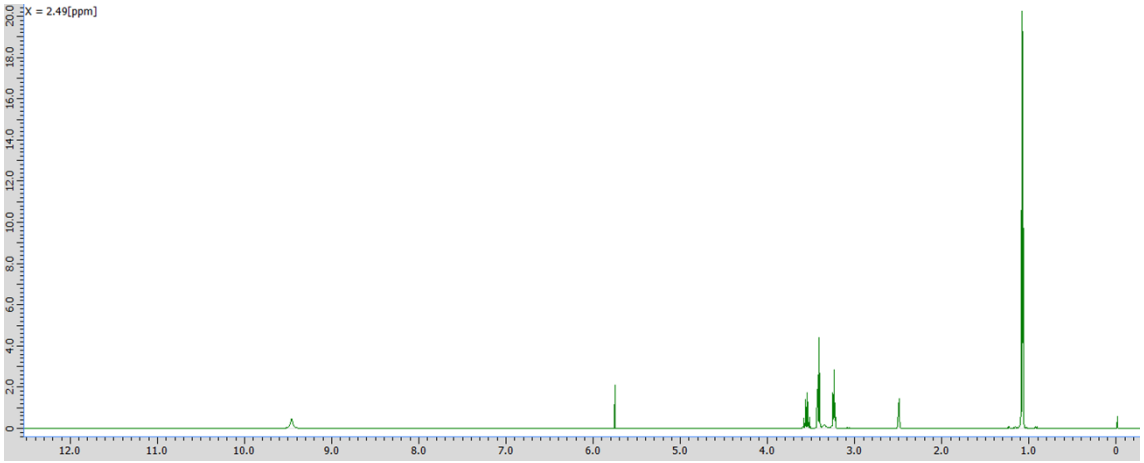

^{13}C NMR

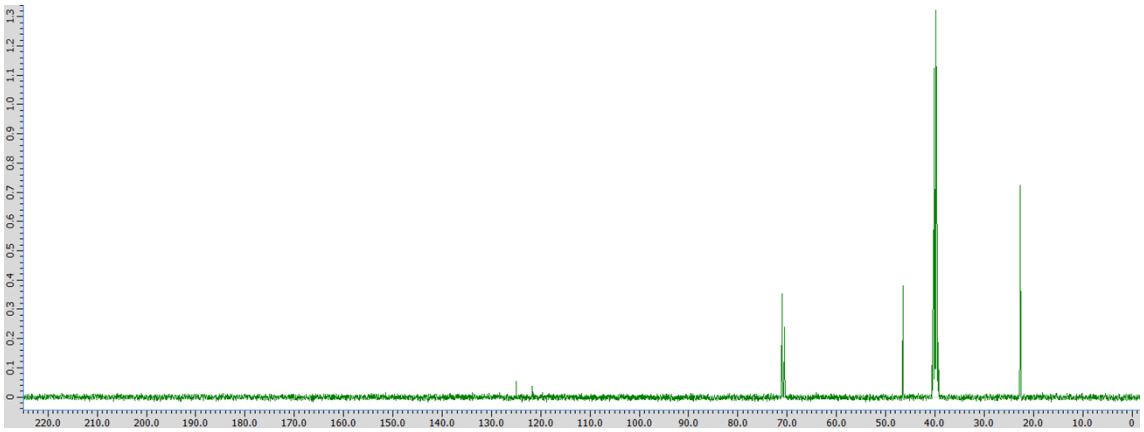

^{19}F NMR

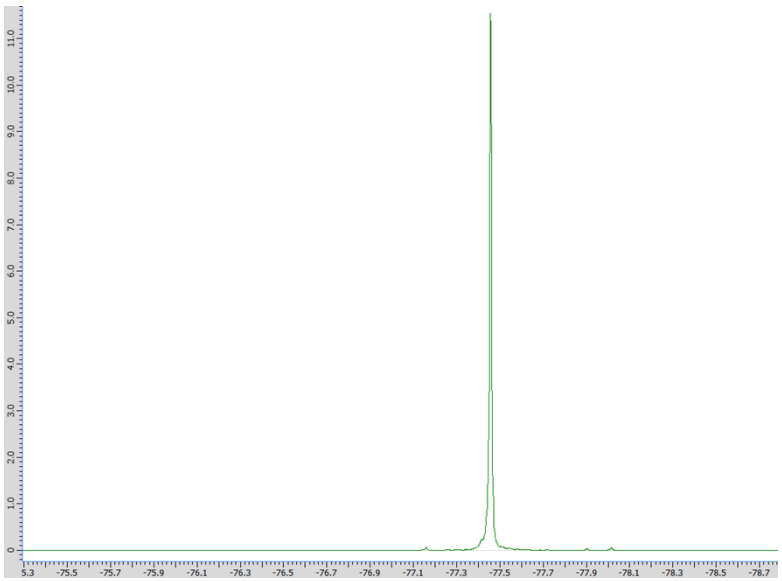

Li[IESI]

^{1}H NMR

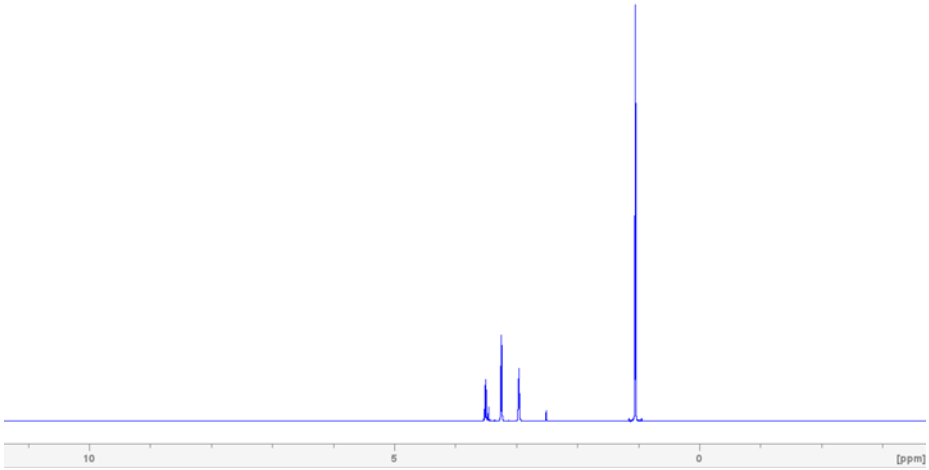

^{13}C NMR

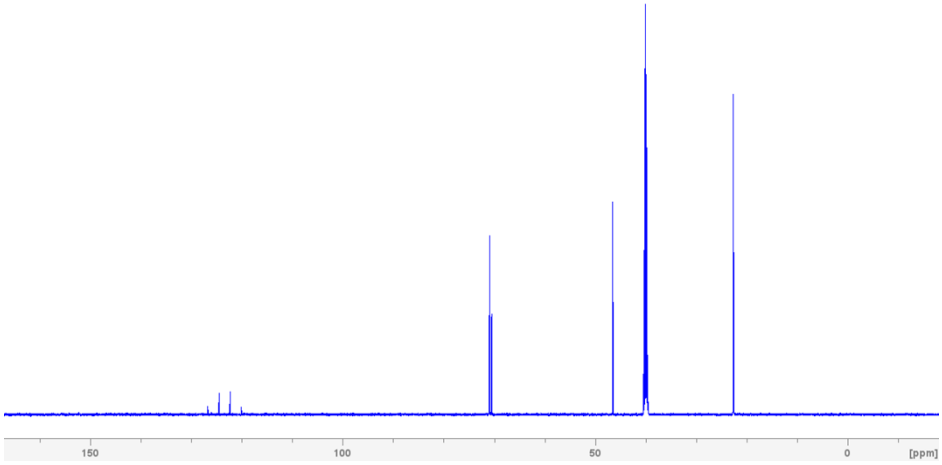

^{19}F NMR

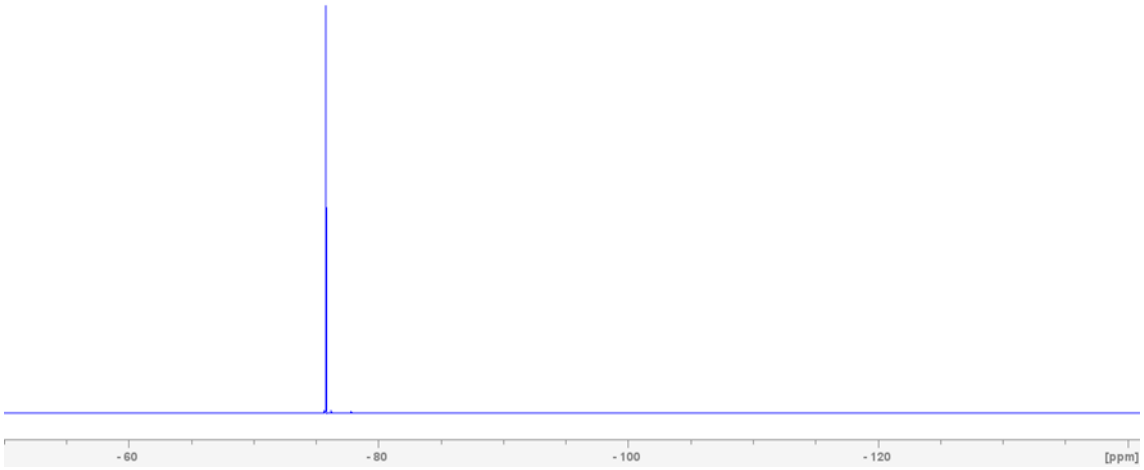

H[ETFSI]

^{1}H NMR

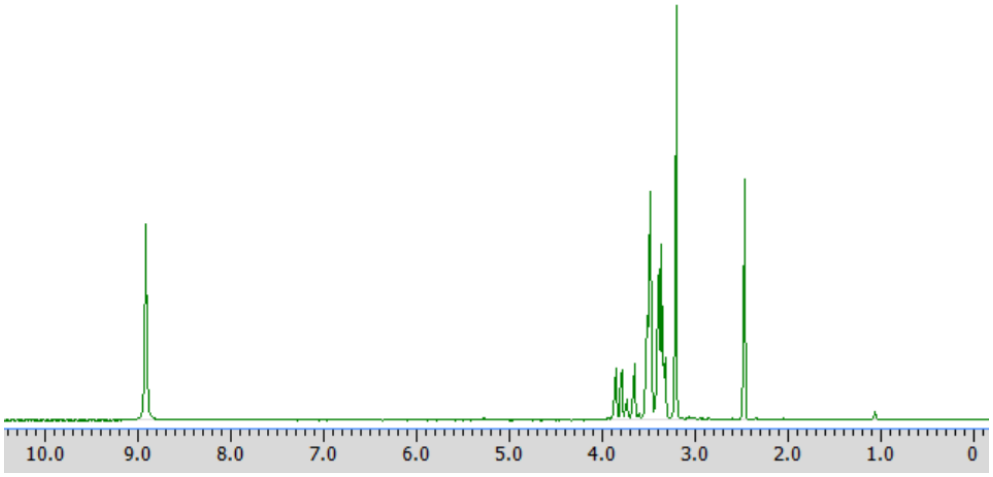

^{13}C NMR

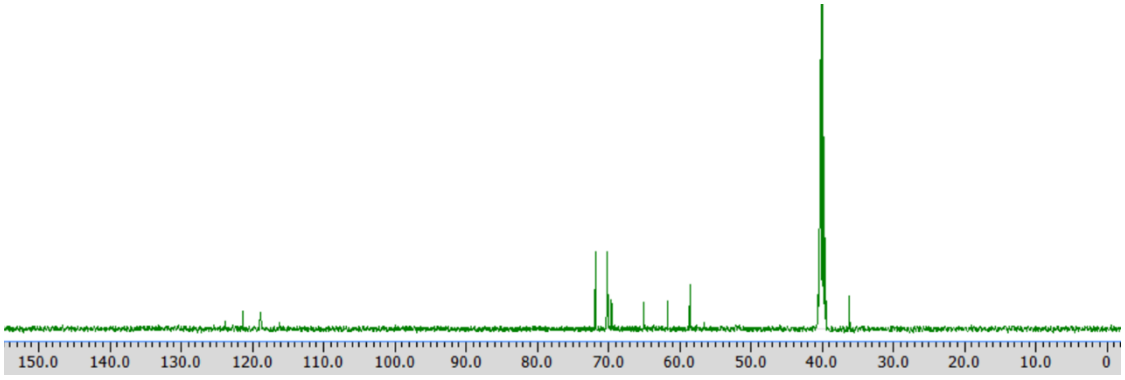

Li[ETFSI]

^{1}H NMR

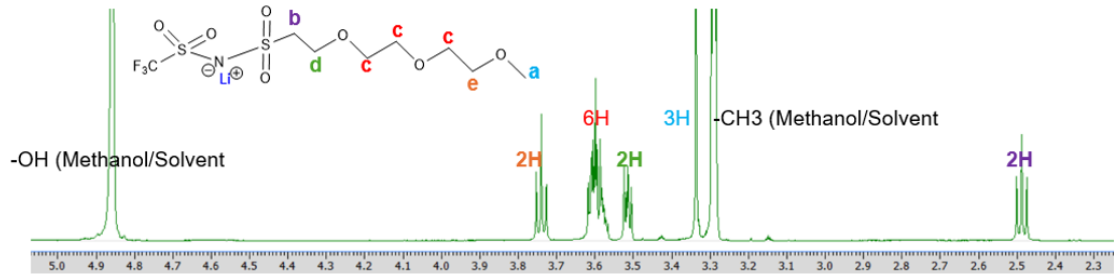

^{13}C NMR

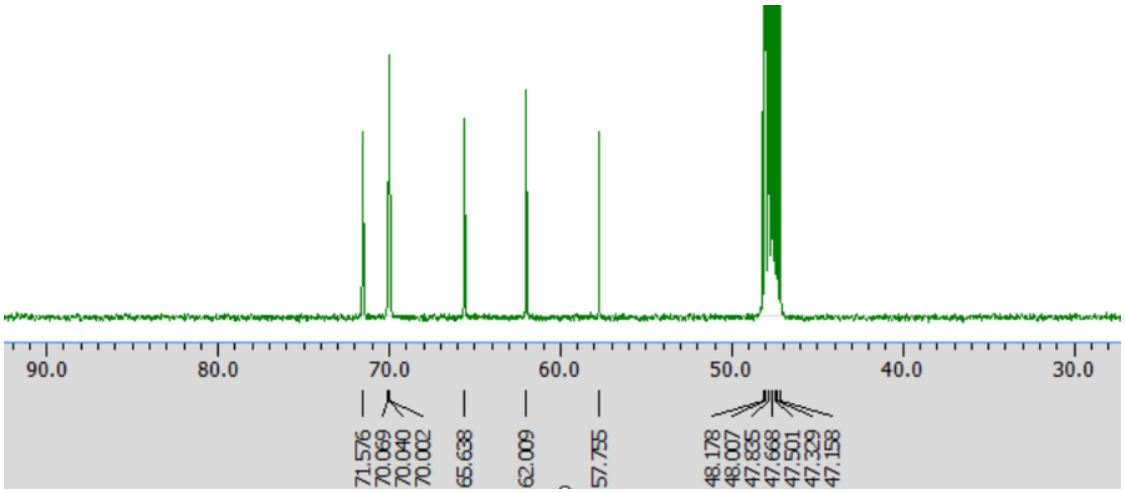

^{19}F NMR

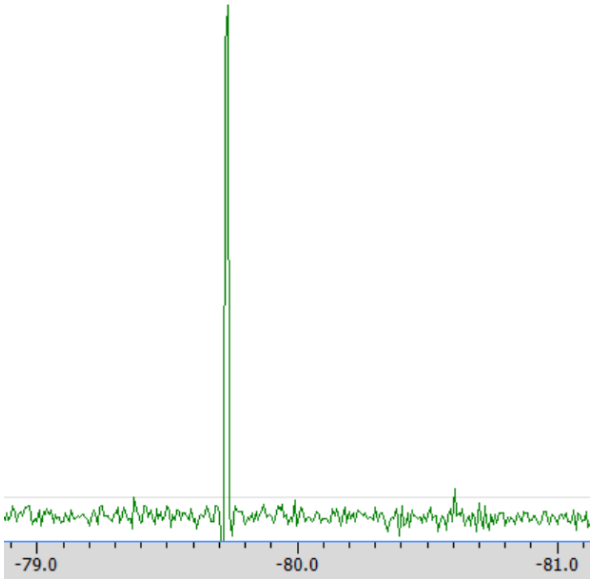

References

1. A. M. Borys, *Organometallics*, 2023, **42**, 182-196.
2. F. Philippi, M. Middendorf, K. Shigenobu, Y. Matsuyama, O. Palumbo, D. Pugh, T. Sudoh, K. Dokko, M. Watanabe, M. Schönhoff, W. Shinoda and K. Ueno, *Chemical Science*, 2024, **15**, 7342-7358.
3. K. Bahrami, M. M. Khodaei and M. Soheilizad, *The Journal of Organic Chemistry*, 2009, **74**, 9287-9291.
4. P. Zhou, H. Zhou, Y. Xia, Q. Feng, X. Kong, W.-h. Hou, Y. Ou, X. Song, H.-y. Zhou, W. Zhang, Y. Lu, F. Liu, Q. Cao, H. Liu, S. Yan and K. Liu, *Angewandte Chemie International Edition*, 2024, **63**, e202316717.
5. in *Solvents and Solvent Effects in Organic Chemistry*, 2010, DOI: https://doi.org/10.1002/9783527632220.ch7, pp. 425-508.
6. B. J. Ransil, *The Journal of Chemical Physics*, 1961, **34**, 2109-2118.
7. S. F. Boys and F. Bernardi, *Molecular Physics*, 1970, **19**, 553-566.
8. S. Tsuzuki, K. Hayamizu, S. Seki, Y. Ohno, Y. Kobayashi and H. Miyashiro, *The Journal of Physical Chemistry B*, 2008, **112**, 9914-9920.